DEVELOPMENT OF AN IN VIVO DOSIMETRY SYSTEM

USING RADIOPHOTOLUMINESCENCE FROM SILVER-DOPED PHOSPHATE GLASS

FOR RADIOTHERAPY APPLICATIONS

By

NISHAN SHRESTHA

Bachelor of Science in Engineering Physics
Southern Arkansas University
Magnolia, AR
2013

Submitted to the Faculty of the
Graduate College of the
Oklahoma State University
in partial fulfillment of
the requirements for
the Degree of
MASTERS OF SCIENCE
December 2017

DEVELOPMENT OF AN IN VIVO DOSIMETRY SYSTEM

USING RADIOPHOTOLUMINESCENCE FROM SILVER-DOPED PHOSPHATE GLASS

FOR RADIOTHERAPY APPLICATIONS

Thesis Approved:

Eduardo G. Yukihara, Ph.D.

Thesis Adviser

Stepehen W.S McKeever, Ph.D.

Sergey Sholom, Ph.D.

ACKNOWLEDGEMENTS

I would like first to thank my thesis advisor Dr. Eduardo G. Yukihara. The knowledge and experience gained while working with him helped me immensely to contribute to this project.

I would like to thank Dr. Stephen McKeever for giving me the opportunity to work with him and being my mentor throughout the project. It was a pleasure working with him and the knowledge and experience I gained throughout the project are invaluable to me.

I wish to thank Dr. Sergey Sholom for helping me with any major or minor questions I had and guiding me throughout the project. I would not have been able to complete my project without him.

It is my pleasure to thank our collaborators, without whom the clinical testing of the technique would not be possible. My gratitude to Dr. David Klein from Oklahoma Cancer Specialist and Research Institute, and Stephen Eller from St. Francis Cancer hospital for taking time out of their busy schedules to help us with the irradiations.

I wish to acknowledge Chiyoda Corp. for their financial support throughout my Masters research, which allowed me to concentrate on the research.

I would also like to thank my lab mates for making the lab a fun filled workplace. I cannot thank them enough for helping me with as small as Excel, Origin shortcuts to crazy discussion, and suggestions regarding my project.

Finally, I must express my very profound gratitude to my parents and to my friends for providing me with unfailing support and continuous encouragement throughout my years of study and through the process of researching and writing this thesis. This accomplishment would not have been possible without them.

Acknowledgements reflect the views of the author and are not endorsed by committee members or Oklahoma State University

Name:	NISHAN SHRESTHA
Data of Degree:	December, 2017
Title of Study:	DEVELOPMENT OF AN IN VIVO DOSIMETRY SYSTEM USING RADIOPHOTOLUMINESCENCE FROM SILVER-DOPED PHOSPHATE GLASS FOR RADIOTHERAPY APPLICATIONS
Major Field:	PHYSICS WITH OPTION IN MEDICAL PHYSICS

Scope and Method of Study: The goal of this project was to determine the potential of using radiophotoluminescence (RPL) from silver-doped phosphate glass as a real-time, in vivo dosimeter in radiation therapy. Our objective is to develop a portable RPL reader and identify the technical difficulties and potential solutions to decide on the feasibility of such system. Two different setups were built to characterize the material luminescence properties, such as the excitation/emission wavelength, to select proper optical filters for the system. The stimulation and detection components of the system were characterized to understand the overall stability of the system. Additional material characteristics, including the dose build up effect, were also studied. Based on these studies a qualitative model for the RPL properties was proposed.

Findings and Conclusions: The results show that that the diode laser when operated in QCW mode is limited by the laser rise and fall time, which needs to be taken in to account when taking time discrimination measurements. There is background fluorescence in the system which reduces the sensitivity and dynamic range of the system. It was also found that the increase in temperature of the RPLGD and laser intensity reduces the RPL intensity with time. However, with use of proper neutral density filters this problem can be resolved. A model based on some of the new findings about the material has been proposed to explain build-up effect, temperature dependence, and UV bleaching effect which were not presented in literature or explained by previous models. The rate of build up was characterized and it was found to be independent of dose or dose rate. Thus, a universal build-up curve can in principle be formulated and used to calculate dose from an irradiated sample based on the readout time.

ADVISER'S APPROVAL: Dr. Eduardo G. Yukihara

TABLE OF CONTENTS

LIST OF TABLES

LIST OF FIGURES

CHAPTER 1

INTRODUCTION

The goal of radiotherapy is to treat cancer without health detriment to the patient, which requires delivery of prescribed dose to various types of tumor safely and accurately. For this purpose, comprehensive Quality Assurance (QA) programs are essential. Nevertheless, a number of radiation incidents have been reported (Derreumaux et al., 2008) and several papers have reviewed treatment errors that were not identified in QA, but could have been avoided by in vivo dose measurements (Mijnheer et al., 2013). As a result, in vivo dosimetry has been used extensively in External Beam Radiotherapy (EBRT) especially in certain treatments like Total Body Irradiation (TBI) and Total Skin Electron Irradiation (TSEI), where the doses need to be measured at different points on the body. In fact, the importance of in vivo dosimetry has been recognized and implemented as a part of QA program in many countries like France, Sweden, Norway, Denmark, and the UK (Derreumaux et al., 2008; Thwaites et al., 2005). To do so, however, small, sensitive, real-time in vivo dosimeters for use during treatment are required.

A good in vivo dosimeter has high accuracy and precision, a linear dose response, a stable signal, and provides immediate results. Diode detectors are one of the most common in vivo dosimeters. However, they perturb the radiation field, the sensitivity changes over time with radiation, and they are energy and temperature dependent (Saini and Zhu, 2004). Metal Oxide Semiconductor Field Effect Transistors (MOSFETs) can also perturb the radiation field, the sensitivity varies with temperature and accumulated dose, and they are energy and dose-rate

dependent (Jornet et al., 2004). Because diodes and MOSFETs perturb the radiation field especially due to the metal electric leads, plastic scintillation detectors (PSD) using fiber optics are also used. In PSDs the electrons generated in the medium by the ionizing radiation recombines immediately emitting photons. Thus, readout can only be made during irradiation. Thus, during irradiation they suffer from the large background due to Cherenkov radiation or "stem effect" (Beddar et al., 1992a). This opens an opportunity for Optically Stimulated Luminescence Detectors (OSLDs), especially Al_2O_3:C, which are found to be energy and angle dependent as well (Aznar et al., 2004). OSLDs, unlike scintillators, have trapping centers that trap the electrons generated during irradiation, which can then be readout with optical stimulation. Thus, OSLDs can be readout between linear accelerator (linac) pulses and are not affected by the stem effect. Due to slow response of Al_2O_3:C, however, another OSL material KBr:Eu was investigated for real time in vivo dosimetry, for which the readout time was tens of milliseconds (Gaza and McKeever, 2006; Klein et al., 2010).

Silver-doped phosphate glass radio photoluminescence detectors (RPLDs) are of interest for medical dosimetry, as they have a linear dose response and wide dynamic range, from 10 μGy up to 10 Gy (Yamamoto, 2011). The Dose Ace System, developed by Chiyoda Technol Corporation (Japan) to read out the RPLDGDs (Araki et al., 2004), is reported to have low energy dependence of <1 % for 6 MV – 10 MV photon beams, and none for higher energies (Mizuno et al., 2008). They also have minimal fading of 1.6 % over 133 days , angle dependence of <1 % over ± 90°, and are dose rate independent within ±2 % (Rah et al., 2009), with a high signal uniformity and reproducibility within 1%.

The goal of this project is to determine the potential of using radiophotoluminescence (RPL) from silver-doped phosphate glass as a real-time, in vivo dosimeter in radiation therapy.

Our objective is to develop a portable RPL reader and identify the technical difficulties and potential solutions to decide on the feasibility of such system. We tested two different setups and characterized the material luminescence properties, such as the excitation/emission wavelength, to select proper optical filters for the system. The stimulation and detection components of the system were characterized to understand the overall stability of the system. Additional material characteristics, including the dose build up effect, were also studied. Based on these studies a qualitative model for the RPL properties was proposed.

CHAPTER 2

BACKGROUND

In this chapter, we discuss the basic RPL mechanism in the silver-doped glass, the importance of in vivo dosimetry, advantages and disadvantages of available in vivo dosimeters, and possible challenges for silver-doped glass.

2.1 In vivo dosimetry

In vivo dosimetry is the most direct method of measuring the radiation dose delivered to the patient during radiation therapy (Mijnheer et al., 2013; Van Dam and Marinello, 1994). In vivo dosimetry is an additional test that complements the Quality Assurance (QA) program that is done before the treatment and gives an independent assessment of the dose to be delivered to the patient and previously calculated from the treatment planning system (Ismail et al., 2009). In vivo dosimetry also helps in accurate dose delivery of conformal radiotherapy (Lanson et al., 1999) and can be useful in finding human errors in treatment planning procedures, the performance of the accelerator, monitor unit calculation program, and the difference in patient geometry between irradiation and planning.

In vivo dosimetry is performed by placing a dosimeter on the patient's skin before treatment. There are two primary purposes of in vivo dosimetry: "entrance dose measurements" and "exit dose measurements". Entrance dose measurements help to identify errors in beam energy, omission or use of wrong accessories, changes in beam output, and

patient setup errors (Howlett et al., 1999; Lee et al., 1994). Exit dose measurements give information on patient thickness and heterogeneities in the anatomy. In addition, in vivo dosimetry is also used for out-of-field measurements in treatments with high dose gradients, which can be useful in assessing organs at risk around the tumor (Duggan and Coffey, 1998; Ramsey et al., 2006).

Although in vivo dosimetry has been found to improve the treatment delivery in different circumstances like TBI, TSEI, and brachytherapy (Cozzi and Fogliata-Cozzi, 1998; Mangili et al., 1999; Mijnheer et al., 2013), whether or not to include in vivo dosimetry in the QA program has been a topic of debate (Feldman and Edwards, 2008). Recent overexposure incidents in Panama and others reported by the media show the importance of in vivo dosimetry during cancer treatments (Bogdanich and Series; Bogdanich and Ruiz, 2010; IAEA, 2001; Vatnitsky et al., 2001), but not every IMRT treatment plans are validated before delivery (Ramsey et al., 2003). Thus, additional steps must be taken to ensure accurate dose delivery (Hendee, 2011; Hendee and Herman, 2011). In vivo dosimetry is not mandatory, but it is an important tool and adds value to a strong clinical QA program (Feldman and Edwards, 2008).

2.2 In vivo dosimetry techniques

A detector must meet several requirements for use in radiation therapy (Van Dam and Marinello, 1994). The first requirement for any detector is to have high sensitivity. In a typical treatment, the dose is ~2 Gy per fraction with out-of-field doses in the 10 mGy range. Thus, the detector should be able to measure ~ 1 mGy to estimate the prescribed dose with an adequate signal-to-noise (SNR) ratio. The detector must have a linear dose response over a wide dynamic range. The detector material should be tissue equivalent or close to it. It should have a small active volume and not perturb the radiation field. The detector should be simple to use, fast and

able to be read on site. Any detector system used in treatment verification must meet all of the above requirements and have the precision of <1% to achieve a 5% accuracy of the mean dose in the target volume (Brahme, 1984).

Currently, there is no single in vivo dosimeter that meets all the requirements of an ideal dosimeter. Different detectors have their own advantages and disadvantages. Diodes, metal-oxide semi-conductor field effect transistors (MOSFETs), and plastic scintillation detectors (PSDs) are some examples of commercially available real-time in vivo dosimeters. Electronic portal imaging devices (EPIDs) are also commercial and provide information that can be used to infer the dose. Some important properties are summarized in the table below.

Table 1. Comparison of available real-time in vivo dosimetry techniques, highlighting their main advantages and disadvantages.

Technique	Advantages	Disadvantages
Diodes	Good reproducibility (Mijnheer et al., 2013)	Dose rate, energy and angle dependent (Saini and Zhu, 2004)
	High sensitivity	Radiation damage
		Perturbs radiation field
MOSFETs	Small size	Response drift after irradiation
	Linear dose response	Dose rate, energy and angle dependent (Jornet et al., 2004)
	Waterproof	Perturb radiation field
		Low precision and accuracy (Scalchi and Francescon, 1998)
		Sensitivity change with dose
OSLD	Good reproducibility	Light sensitive
	Dose linearity	Sensitivity change with accumulated dose (>20 Gy)
	Dose rate independent	Sensitization effects with optical bleaching
	Energy and angular independence	
PSD	Water equivalent	Stem effect (Beddar et al., 1992b)
	Dose linearity (Beddar et al., 1992b)	Energy dependence
	Resistance to radiation damage	
	High resolution	

The main advantage of using silver-doped glass as a real-time in vivo dosimeter is the fact that the readout is non-destructive. Thus, the detector can be read multiple times without loss of signal. Typically, in vivo dosimeters are not stored for the record, but, with the added benefit of re-reading, the medical physicist can catalogue the detector with the patient chart for posterior re-evaluation, if necessary. The disadvantage is that the signal cannot be reset without removing the probe and annealing to a temperature of ~400 °C (Miyamoto et al., 2011).

2.3 Radiophotoluminescence

RPL is a luminescence phenomenon. The technique was first described in the early 1950s and was applied to measurements in accident dosimetry (Schulman et al., 1951). In RPL materials, the periodicity of the perfect crystals is violated by introducing defects (e.g., missing ions, extra ions, etc., in the lattice points). These defects in the crystal undergo radiochromic transformation, creating specific RPL centers with different optical properties than that of the original defects.

Figure 2-1 illustrates the RPL process for a hypothetical material with one luminescent defect. Upon irradiation, the newly created charges are trapped in the defects. These defects exhibit luminescence and have characteristic absorption and emission spectra. Once the charges are captured by the defects, they undergo a radiochromic transformation and RPL centers are created. These centers have their own optical properties such as absorption, excitation and emission bands compared to the defects. Once the RPL centers are created, the electrons can be excited (in case of silver-doped glass with UV light) to a higher energy level, which is a metastable state. Thus, the electron relaxes back to the ground state with emission of fluorescence light in the visible range.

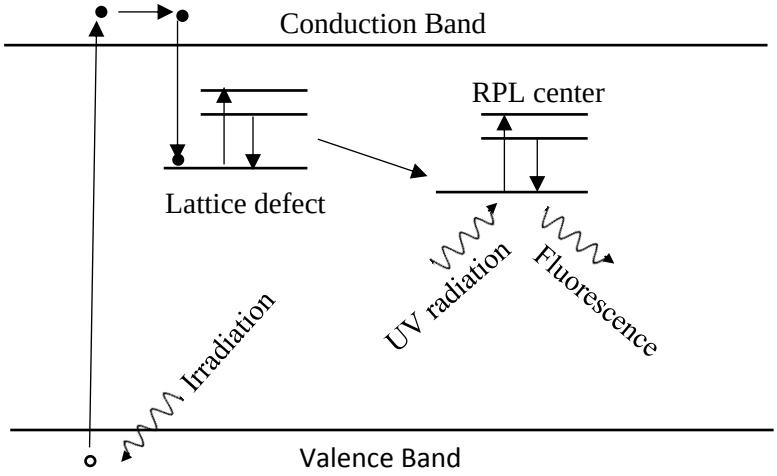

Figure 2-1. Schematic diagram for RPL trap formation, excitation, and fluorescence. Reproduced from Perry (1987).

2.4 RPL from silver-doped phosphate glass

Silver-doped phosphate glass is a well-known RPL material (Yokota and Imagawa, 1967). The glass has high radiosensitivity and repeatability for radiation measurements; thus, it can be used as an integrating type of dosimeter for individual and environmental dosimetry (Maki et al., 2011).

When the glass is exposed to ionizing radiation, electron-hole pairs are produced. According to the standard model described in the literature (Miyamoto et al., 2011), the liberated electrons and holes are then captured in the Ag^{+} sites, creating Ag^{0} and Ag^{++} ions. Both the Ag^{0} and Ag^{++} centers are RPL centers (Yokota and Imagawa, 1967). We will see later in this thesis that this model may not account for all luminescence processes observed in the silver-doped glass.

$$Ag^{+} + e^{-} \rightarrow Ag^{0} \quad \textbf{(2.1)}$$

$$Ag^{+} + h^{+} \rightarrow Ag^{++} \quad \textbf{(2.2)}$$

As shown in Figure 2-2, there are three excitation bands, after irradiation, in the UV region peaked at 315 nm attributed to Ag^{++} ions (Equation 2.1) and 360 nm due to Ag^{0} ions (Equation 2.2). In addition, due to the two centers Ag^{0} and Ag^{++}, the glass has two emissions bands. The 460 nm (blue) emission is attributed to the Ag^{0} center, whereas the 560 nm (yellow) emission is attributed to the Ag^{+} center. These RPL centers can, however, be destroyed by thermal annealing at 400 °C for 20 min for doses <1 Gy, and for 60 min for doses >1 Gy (Miyamoto et al., 2011). Later in this work we will re-examine these band attributions.

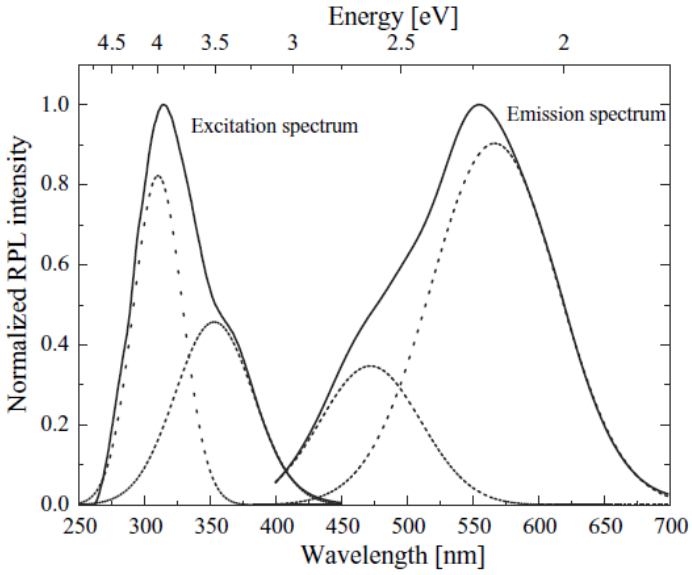

Figure 2-2. RPL emmision and excitation spectra of the glass dosimeter after X-ray irradiation. (Miyamoto et al., 2010a)

Figure 2-3 shows the energy band diagram of RPL centers in the silver-doped glass, with Ag^{0} and Ag^{++} ions along with the PL center due to Ag^{+} ions. As shown with UV excitation, the

electrons in the Ag^0, Ag^+, Ag^{++} centers can be excited to the higher energy level, which is metastable. Thus, the electrons relax back to their initial stable state with the release of visible light. From the proposed model, Ag^0 is responsible for the blue RPL emission at 460 nm, Ag^+ for PL at 302 nm, and Ag^{++} for yellow RPL at 560 nm. The lifetime of the blue emission is <10 ns and the lifetime of yellow emission is <4 µs (Miyamoto et al., 2010b).

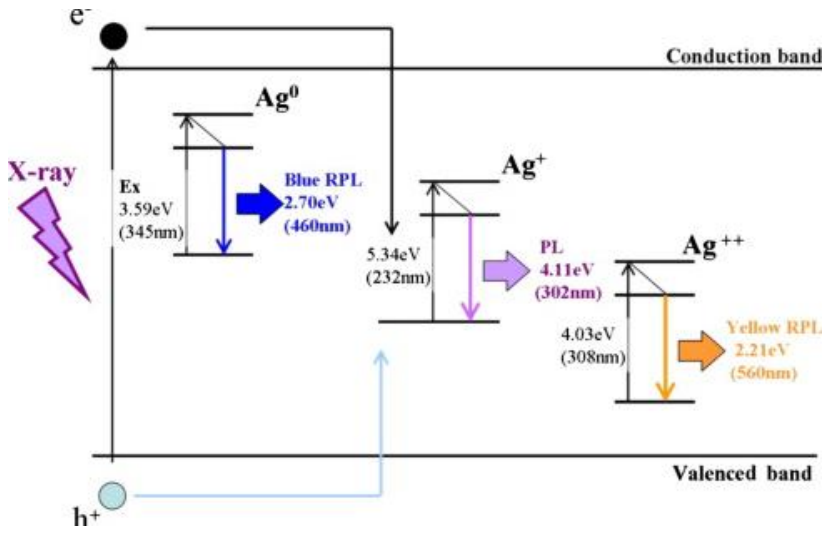

Figure 2-3. Band diagram model of RPL emission for silver-doped phosphate glass (Miyamoto et al., 2011).

One challenge of using RPL glass detectors (RPLGDs) is the build-up effect (Miyamoto et al., 2011; Perry, 1987; Yokota and Imagawa, 1967). The primary RPL emission does not stabilize immediately after irradiation, showing instead a period of slow growth ("build-up") following irradiation. Figure 2-4 shows clearly the build-up effect, where the orange RPL signal increases with time. It has been found that heating the sample at 70°C for 30 minutes after irradiation accelerates the build-up effect.

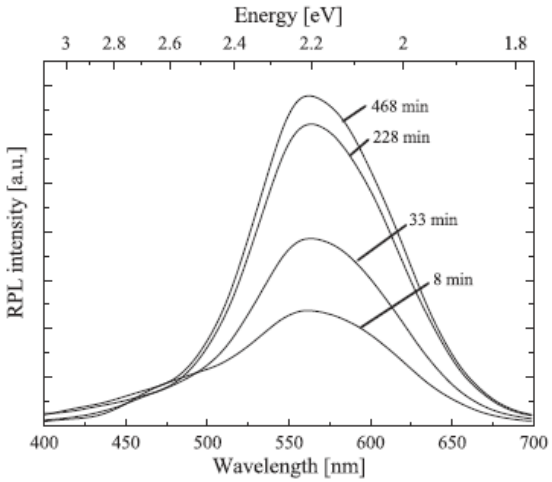

Figure 2-4. Growth of RPL with time after irradiation in RPLGD (Miyamoto et al., 2010a).

The RPLGD's are commercially used for personal monitoring, environment monitoring, and medical dosimetry. There are three major types of RPL glass dosimeters as shown in Figure 2-5. The SC-1 dosimeters are used for environment dosimetry, the GD-450 for personal dosimetry, and GD-300s for medical dosimetry.

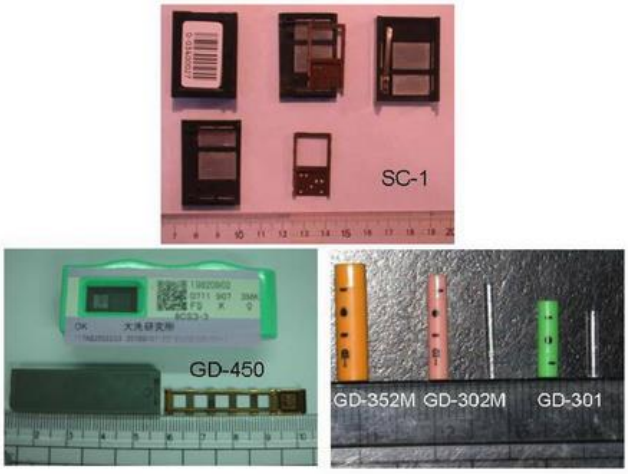

Figure 2-5. Three types of RPLGD: the SC-1 system for environmental radiation monitor, the GD-450 for personal dose monitor, and the GD 300s for medical dosimetry (Huang and Hsu, 2011).

Commercial readers for the readout of the glass dosimeters is manufactured by Chiyoda Technol Corporation. Figure 2-6 shows some of the available RPL glass readers: the FGD-202 reader is used for environment dosimetry, the FGD 1000 reader for medical dosimetry, and the FGD 660 reader for personal dose monitoring.

Figure 2-6. Different commerical RPLGD readers, FGD-202 (left), FGD-1000 (right), FGD-660 (below) (AGCGlassCorp, 2007)

The fluorescent components of the RPL glass have been found to consist of three components: the pre-dose component with short decay lifetime (presumably due to dirt), the RPL component, and the pre-dose component with long decay. Due to difference in lifetimes, time discrimination techniques have been used to separate the pre-dose components from the main RPL signal, as shown in Figure 2-7. Figure 2-7 shows that the emission from a RPLGD consists of 3 components. The pre-dose with the long decay component is present in any unexposed samples. After irradiation, the RPL signal is present on top of the pre dose signal. In addition, if any dirt is found in the sample, then the signal will show up on top of the other two components signal. In the decay curve, due to different life times of the components, the signal in the first few 2 μs consists of all the 3 components. However, due to the short lifetime of the pre-dose component, it decays within the first 2 μs leaving behind the RPL and the long decay component. The RPL component decays faster than the pre dose component leaving behind the long decay pre-dose signal.

Table 2. Fluorescent decay components of the silver-doped glass.

Fluorescent component	Lifetime of decay
Pre-dose component (dirt)	~ 1 μs
RPL	~ 40 μs
Pre-dose with long decay	~ 1 ms

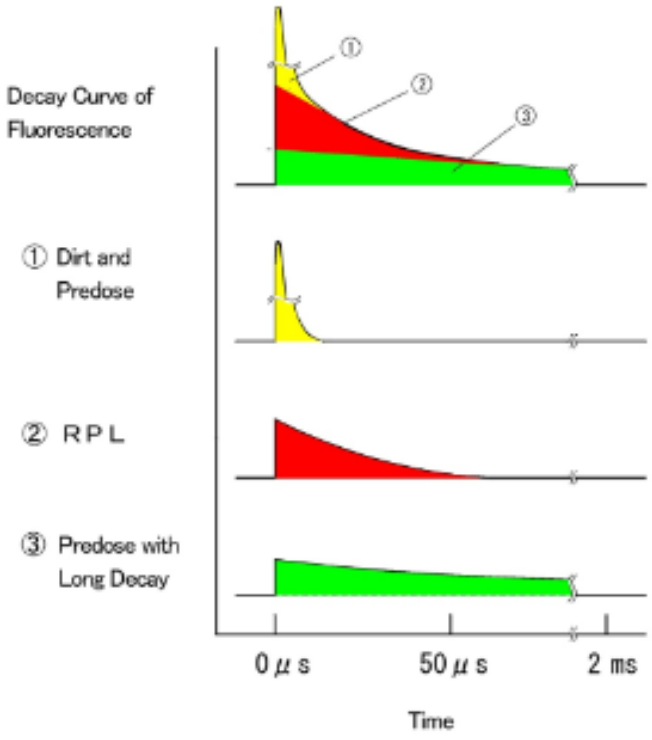

Figure 2-7. Different fluorescence components of the RPLGD (Huang and Hsu, 2011).

The commercial Dose Ace dosimetry system (Figure 2-6) has been used in a variety of areas in medical dosimetry, including postal dosimetry audits of radiotherapy beams (Mizuno et al., 2008), dosimetry in small fields of Cyberknife and Gamma-knife (Araki et al., 2003; Araki et al., 2004; Perks et al., 2005), diagnostic imaging (Knežević et al., 2011), high energy photon and

electron beam radiotherapy (Son et al., 2011), in vivo dosimetry in total body irradiation (TBI) (Rah et al., 2011), and proton beam therapy (Rah et al., 2012).

CHAPTER 3

MATERIALS AND METHODS

This chapter discusses the general experimental details of the studies presented in this dissertation. Details include the detector physical properties, irradiation sources, readout equipment and data acquisition methodologies.

3.1 Samples

The samples used studied in this work are commercially available GD-300 series dosimeters provided by Chiyoda Technnol Corporation, Japan. The samples were approximately 12 mm × 1 mm. Although this size can be considered as large for in vivo dosimetry, the goal of this project is to obtain a proof-of-principle for the technique. Smaller probes will be tested in the future.

Figure 3-1 Image of the samples (GD 302M) used in the studies.

3.2 Annealing

The RPL post-irradiation and pre-irradiation annealing was performed in an electric furnace (Model LMF-3550, Omegalux). To remove any previously accumulated dose, the samples were placed on an annealing magazine and inside the oven at room temperature. The oven was then set to heat up with a linear heating rate of 40 °C/min to 400 °C. The samples were left in the oven for ~60 min at the set hold temperature of 400 °C, and then allowed to cool naturally.

3.3 Irradiations

Laboratory irradiations were performed using a 250 mCi $^{90}Sr/^{90}Y$ beta irradiator (~0.4 Gy/s, ~10 cm source-to-sample distance). The samples were irradiated individually one at the time. It should be noted that the dose delivered from the source is not uniform throughout the samples. Figure 3-2 shows the dose distribution in x and y direction away from the point of the maximum dose, measured using OSL films (Ahmed et al., 2017). This shows that the samples positioning can affect the total dose received by them. Thus, to improve sample position reproducibility, a paper mask was used to place the samples in the source during irradiation.

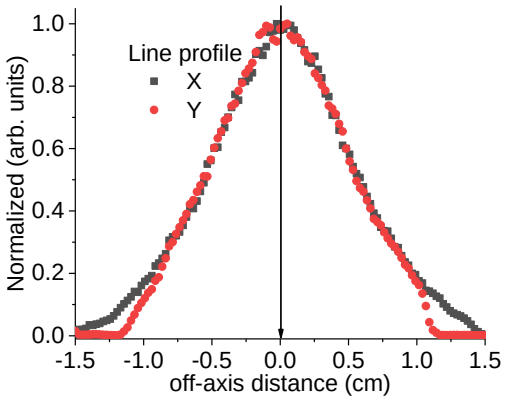

Figure 3-2. Dose distribution in the $^{90}Sr/^{90}Y$ beta souce measured using the OSL films and 2D dosimetry system (Ahmed et al., 2017).

To obtain the RPL spectrum, some samples were also irradiated in a dual cabinet X-ray system (model 43805N, Hewlett Packard, Inc.) with 30 kV energy at 2.2 mA current for 5 min.

Irradiations with 6 MV photon beam were performed using a Varian 2100EX linear accelerator at the St. Francis Hospital (Tulsa, OK). The RPLGDs were placed in a plastic water phantom, at 1.5 cm depth in a 100 cm source-to-surface distance (SSD) setup. The field size used was 15 cm × 15 cm. For linearity check, an ionization chamber was placed at 10 cm water equivalent depth during all irradiations. The samples were irradiated with 1, 3, 10, 30, 100, 300, 1000 monitor units (MU). The doses were calculated using the MU to dose-to-water conversion factor measured on the same day. All irradiations were performed under regular room light.

3.4 In vivo dosimetry system

3.4.1 Laser diode setup

Two different setups were built: the first prototype here called the “laser diode setup”, utilizes a laser diode which can be operated in Continuous Wave and Quasi Continuous Wave

(QCW) mode. In QCW mode, the laser can be operated in pulsed mode with pulse width range of 100 µ - 1 s and frequency of 0.2 – 1000 Hz. Two different types of the detector were tested in the first prototype: an avalanche photodiode (APD) and a photomultiplier tube (PMT). A PMT was used because the current APD was not fast enough to perform time resolved measurements. In both setups, the system consisted of a stimulation unit and a detection unit coupled to an optical fiber, with the distal end of the fiber coupled to an RPLGD.

Figure 3-3 shows the schematics of the "laser diode setup". It consists of a laser diode (model L375P70MLD, 70 mW output power, ThorLabs, Inc.) mounted in a temperature-controlled laser mount (model TCLDM9, ThorLabs, Inc.) for stimulation. The laser beam was focused by a series of lenses through a 375 nm laser line filter (Stock #86-736, Edmund Optics Ltd.) onto the input of the optical fiber. The laser then passes through a short-pass dichroic mirror (Stock #69-214, Edmund Optics Ltd.) into the proximal end of a silica fiber. The RPGLD was mounted at the distal end of an optical fiber (model OCF-103604, 1.15 m length, 1000 µm core diameter, Ocean Optics, Inc.). The laser stimulates the sample and the RPL signal is guided back along the fiber to the short-pass dichroic mirror, where it is reflected into the APD (model APD 120A, 1 mm active diameter, Thorlabs, Inc.), through a 600 nm long-pass filter (model FEL0600, Thorlabs, Inc.), a 700 nm short-pass filter (Stock #47-291, Edmund Optics Ltd.) and a 405 nm long-pass filter (model BLP01-405R-25, Semrock, Inc.). The APD signal was digitized using a data acquisition (model NI USB 6212, National Instruments Co.).

To perform time-resolved measurements, a PMT (model H10721, 8 mm effective diameter, Hamamatsu Co.) was used. The signal from the PMT was digitized using a dual-channel gated photon counter (model SR400, Stanford Research Systems, Inc.). These measurements were done using the QCW mode of the laser, with a laser pulse width of 0.1 ms

and period of 1 ms. During measurements, the trigger output signal from the laser controller was used to trigger the photon counter's gate. The gate width of 1 µs was chosen. The SR400 photon counter was operated in 'A FOR PRESET T' mode. At the end of the laser pulse, the A-counter counts the photon which occurs during the 1 µs gate. The T-counter is preset to count 10000 triggers, so that the counts will be accumulated to improve SNR. After each data point is taken, the photon counter advances the A-gate by 1 µs, resets the A-counter, and starts the next count interval.

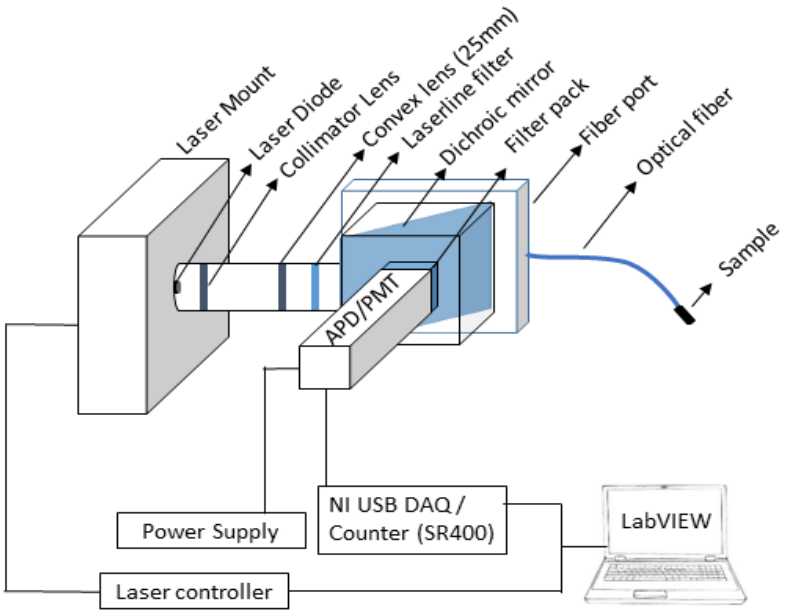

Figure 3-3. Schematic of the "laser diode" optical fiber in vivo dosimetry system with QCW laser.

3.4.2 Pulsed laser setup

The second prototype, here called "pulsed laser setup" and which is the final setup used in these studies, consisted of a pulsed UV laser (model 1Q355-2, 5 µJ output power, pulse duration < 1 ns, repetition rate 10 kHz, CryLas GmbH) as a stimulation unit, and a PMT (model

H10721, 8 mm diameter, Hamamatsu Photonics, Inc.) as a detection unit. The laser frequency and pulse width can be modulated using an external pulse generator. This setup was used only for time resolved measurements and, thus, the APD was not used.

The schematic of the pulsed laser setup is similar to the one shown in Figure 3-3. The difference is that the lenses to collimate the beam were removed, as the pulsed laser beam was already collimated. In addition, a different laser line filter (model FLH355-10, Thorlabs, Inc.) was used.

3.4.3 Lifetime measurements

Lifetime measurements were performed using the pulsed laser setup (Section 3.4.2). The RPLGD's were placed at the distal end of the optical fiber. The pulsed laser was operated at a frequency of 10 kHz. The SR400 photon counter was operated in 'A FOR PRESET T' mode. The external trigger from the pulsed laser was used to trigger the A gate. The A-gate was set in scan mode with a step size of 1 μs and the gate width of 1 μs. Thus, at the end of the laser pulse, the A-counter counts the photons which occur during the 1 μs gate. The T-counter is preset to count 10000 triggers, so that counts will be accumulated for 0.1 s to improve SNR. After each data point is taken, the photon counter advances the A-gate by 1 μs, resets the A-counter, and starts the next count interval. The number of counting periods was chosen to be 90, so the counting stops after the 90 data points have been collected. These 90 data points correspond to the lifetime decay from the RPLGD (one point per μs).

Figure 3-4 shows the time profile for the used to measure the lifetime of the RPL from the glass. The gate width is 1 μs for every counting period *N*, while the gate delay is 0 μs for the first period (*N* = 1). The A gate was open for 1 μs after the falling edge of the laser trigger. Then

the gate is off and the next laser trigger opens the gate again with zero delays. In this experiment, the counts are accumulated for 10000 laser triggers. Then in the next period (*N* = 2), the SR400 photon counter adds a 1 μs delay at the end of the laser trigger and opens the gate. In the same way, signal is collected for 90 counting periods, which corresponds to 90 data points, where each data point represents a time delay of 1 μs after the laser pulse.

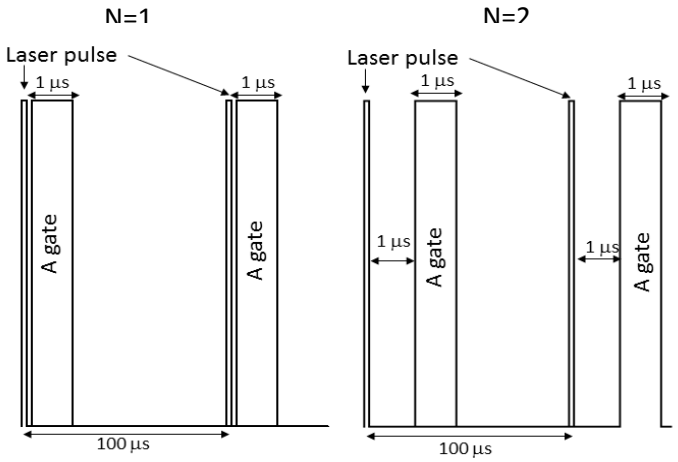

Figure 3-4. Temporal profile of laser pulses and gating.

3.5 Other equipment

3.5.1 Ocean Optics Spectrometer

Spectral measurements were acquired using a fiber optic spectrometer (model USB2000, Ocean Optics, Inc.) shown in Figure 3-5.The USB2000 is a small plug-and-play spectrometer. It is UV-enhanced and equipped with an optical fiber with core diameter of 300 μm, 600 line/mm grating blazed at 300 nm and a 1000 μm × 100 μm slit. The optical resolution of the device depending on the configuration can be varied from 0.1 – 10 nm FWHM. The spectrometer uses a 2048-pixel CCD array where each pixel size is 14 μm × 200 μm with pixel

well depth ~62,500 electrons. The detector range is from 200-1100 nm. It has a signal-to-noise ratio of 250:1 at full signal and Analog-to-digital (A/D) resolution of 16 bit.

Figure 3-5. A USB2000 spectrometer (Ocean Optics, Inc.)

The spectrometer is operated using a commercial software Spectra Suite from Ocean optics. The software allows varying different parameters for measurements like integration time, box car width, number of scans to average. The integration time is the length of time the data is collected. The software allows integration times of 1 ms to 65 s. By using longer integration times, we improve the signal to noise ratio (SNR) by accumulation more signal at the cost of longer readout times. One can also increase the number of scans to reduce the noise on the spectrum.

The response of the detector is wavelength dependent, and the appropriate correction factors should be used to account for this feature, as shown in Figure 3-6. The correction factors were obtained from measuring the spectrum of a NIST-calibrated tungsten light source (Stock #63350, 1000 W, 250 – 2400 nm, Newport Corp.) operated at a fixed current (8.2 A) and with known emission characteristics.

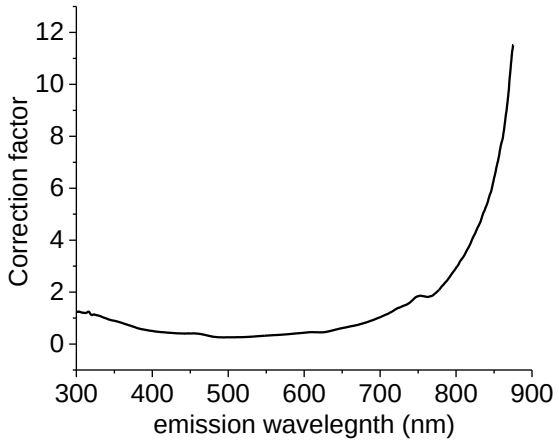

Figure 3-6. Correction factors applied to emission spectra as a result of detector spectral responsitivity.

3.5.2 Dose Ace System

Some of the material characteristic measurements were performed with the commercial RPL glass dosimetry system (Model FDG 1000, Asahi Techno Glass Corp), as shown in Figure 3-7.

Figure 3-7. Automatic RPLGD reader FDG-1000 with an open cover.

The system consists of a stimulation unit, which is a 349 nm N_2 gas laser (repetition rate 20 Hz, pulse width <5 ns, CryLas). The UV laser beam is collimated using a convex lens and filtered using a UV band pass filter of wavelength 349 nm. The filtered laser is split into two beams using a beam splitter, where one beam is directed toward a sample glass, and the other to a reference glass. Once the sample is stimulated, the fluorescence signal is transmitted through the lens and filters, and then collected by the PMT. The reference glass, whose fluorescence is detected using a photodiode, is used to correct for any laser fluctuation. The signal generated by the PMT is pre-amplified and digitized.

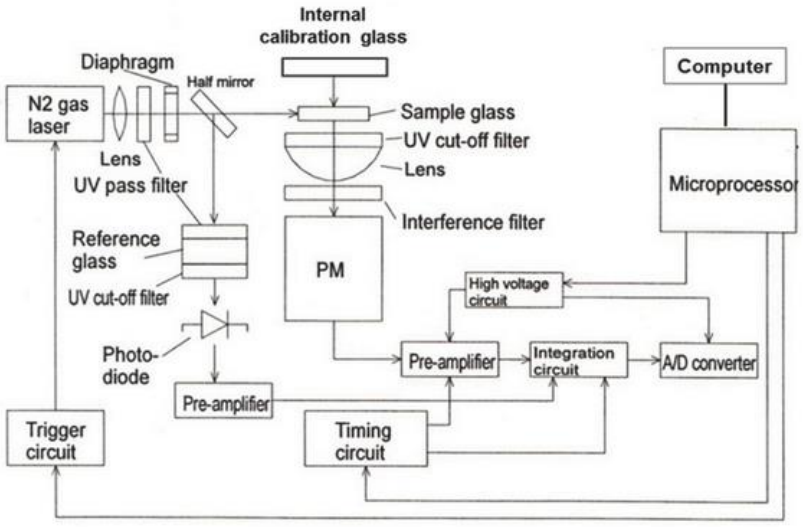

Figure 3-8. Schematic representation of FGD-1000 reader (AGCGlassCorp, 2007).

In the FGD-1000 reader with the UV pulse excitation, the generated fluorescence signal is a combination of both a pre-dose signal (Section 2.4) and the RPL signal. Electronic discrimination between these signals is achieved based on the differences in their decay times, as shown in Figure 2-7. At the end of the laser pulse, the RPL emission at 2 – 7 μs (t_1) and the long pre-dose signal at 40 – 45 μs (t_2) are measured using timing circuit triggers. The RPL signal can then be calculated by:

$$M = I(t_1) - fps * I(t_2) \quad \textbf{(3-1)}$$

where *M* is the readout value, $I(t_1)$ is the RPL intensity, $I(t_2)$ is the intensity of the long pre-dose decay, and fps is the correction factor for the late pre-dose component of the emission.

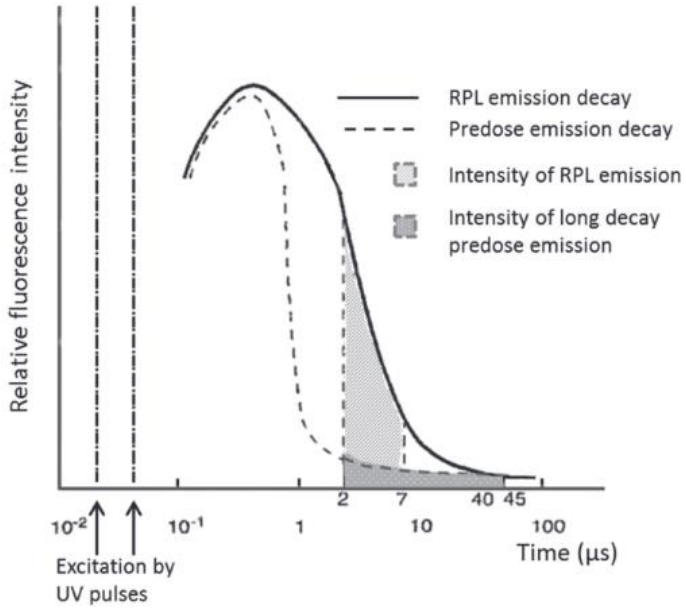

Figure 3-9. Schematic representation of UV pulse excitation, predose and RPL emission with time (Sato et al., 2015).

3.5.3 Optical Absorption

Optical absorption measurements were performed using a Cary 5000 UV-Vis-NIR spectrophotometer (model Cary 5000, Varian) as shown in Figure 3-10. The spectral range of the spectrometer is 175 nm to 3300 nm.

Figure 3-10. Cary Varian 5000 UV/Vis/NIR spectrophotometric equipment.

3.6 Other testing equipment

In addition to the equipment mentioned above, the following components were also used during these investigations.

A Green (532nm) laser diode (100 mW output power, <1% stability, model GMLN-532-100FED, Lasermate Group, Inc.) was used to stimulate the samples for the tests in Section 5.3.2

A UV lamp (Model 3UV-34 UV Lamp, output 4 W) was used to bleach the RPLGD in Section 5.5 to characterize UV bleaching effects.

A Power meter (Model 1918-C, Newport Corp.) was used to measure the output from the UV lamp used to bleach the RPLDGD in Section 5.5.

CHAPTER 4

PRELIMINARY SYSTEM CHARACTERIZATION

In this chapter, we report the preliminary characterization of the RPL signal using the two custom build setups in lab. In addition, characterize the various components of the setups including the stimulation and the detection unit.

The results show the presence of temperature dependence on the RPL signal due to stimulation intensity, which requires further characterization. The diode laser when operated in QCW mode has laser rise and fall time, which needs to be taken in to account when taking time discrimination measurements. The PMT requires some long warm up time before it stabilizes and the pulse laser fluctuation is within 2% thus, monitoring the laser power may improve RPL signal reproducibility. However, the RPL signal was found to vary slightly more than the laser, which we believe might be due to jitter in the timing pulses of the SR400 photon counter.

4.1 RPL signal

This experiment compares the RPL signals from an irradiated and from an un-irradiated glass using the two different setups described in Sections 3.4.1 and 3.4.2.

4.1.1 Laser diode setup

This first test was performed using the system described in Section 3.4.1, based on a laser diode. Two samples, one un-irradiated and one irradiated with 30 mGy (6 MV photons), were stimulated in CW mode and QCW mode. In both modes, the laser was operated at 110 mA current and an APD was used for light collection.

In CW mode the laser in continuously on and the signals were averaged over 1 s. Figure 4-1a show the RPL signal from the un-irradiated and irradiated samples. There is a significant background for the un-irradiated sample and the signal from the irradiated samples is only 2.5× larger than the signal from the un-irradiated sample. A simple estimation shows that the background signal is equivalent to a dose of ~12 mGy, demonstrating a lack of stability of the system. Furthermore, a slow decay of the signal can be observed over the 1 min readout which may be speculated at this point as being the due to warming of the samples under continuous stimulation.

In QCW mode a pulse width of 0.1 ms and 1 ms period was used for stimulation of the two samples. Figure 4-1b shows the RPL signal from the un-irradiated and irradiated sample. The RPL signal is present only when the laser is on and the average signal over the 0.1 ms laser pulse width is the RPL signal. The background from the un-irradiated samples is comparable to the CW case.

In conclusion, we found that in both CW and QCW modes the RPL signal is not stable, decreasing with readout time. This requires further investigation.

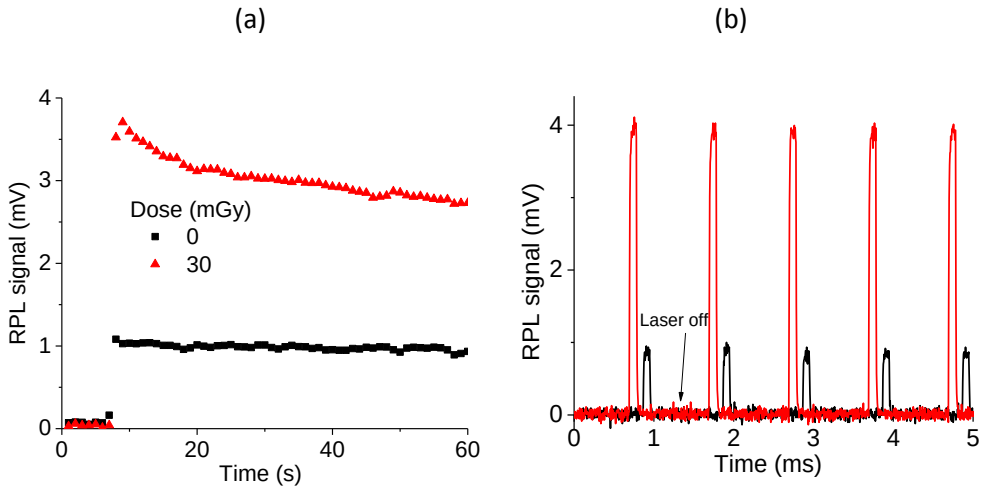

Figure 4-1. RPL signal from an irradiated and non-irradiated glass with laser stimulation in (a) CW mode and (b) QCW mode.

4.1.2 Pulsed laser setup

Tests were performed using the system described in Section 3.4.2 to try to improve the discrimination between the background and RPL signal using time-discrimination. Two samples, one un-irradiated and one irradiated with 10 mGy (6 MV photons), were stimulated using a pulsed UV laser. The output pulse from the laser was used to trigger the SR400 photon counter. The counts were accumulated using 10000 laser pulses where each period is equivalent to 1 s. After each measurement, a delay of 1 μs was added between the end of the laser pulse and the start of the SR400 photon counter.

Figure 4-2 shows the RPL signal from an irradiated and un-irradiated glass with a pulsed laser as a function of the delay between the laser pulse and SR400 photon counter. The RPL signal from a pulsed UV excitation is similar to Figure 2-7, where the huge signal immediately after the laser pulse is the pre-dose PL signal, most of which decay within the first microseconds. After the first microsecond, the background signal from the un-irradiated sample decays significantly by ~85 %, whereas the RPL signal is reduced by only ~50 %. If the signal between 2

and 7 μs is integrated, the background signal corresponds to ~ 1 mGy. There is, however, still a long-decaying background signal corresponding to a dose of ~0.2 mGy, as also shown in Figure 4-2.

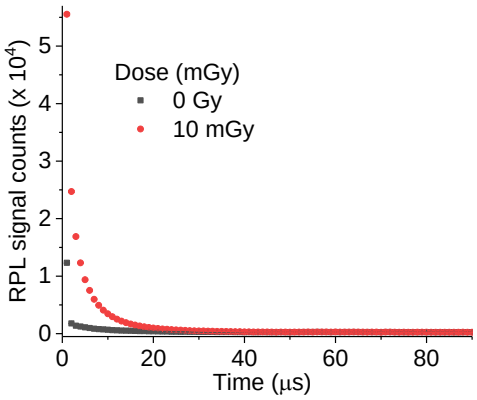

Figure 4-2. RPL signal from an irradiated and a non-irradiated glass with pulsed laser stimualtion as a fucntion of time after the laser pulse.

4.2 Test of the Thorlabs diode laser in QCW mode

To better understand the possibility of using the diode laser setup for time discrimination measurements, it was important to characterize the behavior of the laser pulse of the laser diode setup (Section 3.4.1) in QCW mode. The laser itself has relatively slow switch-on and switch-off times. To measure this, the output of laser pulses, with a pulse width of 0.1 ms and a 1 ms period, were monitored directly for different laser currents using the PMT. Neutral density filters with a total optical density (OD) of 1.0 and a variable aperture in front of were used to avoid PMT saturation.

Figure 4-3a shows the shape of a single laser pulse with pulse width of 0.1 ms for different laser currents. Figure 4-3b and c shows the rise and fall of the laser pulses. The switch-on time is slower than the switch-off time and is laser power (current) dependent. The switch-

on time for a laser current of 50 mA is ~ 18 µs and 8 µs for 110 mA. However, the switch-off time is very rapid and independent of laser power and is ~2 - 3 µs. This is critical for time-discrimination measurements, where the switch-off time limits the beginning of the RPL signal measurement.

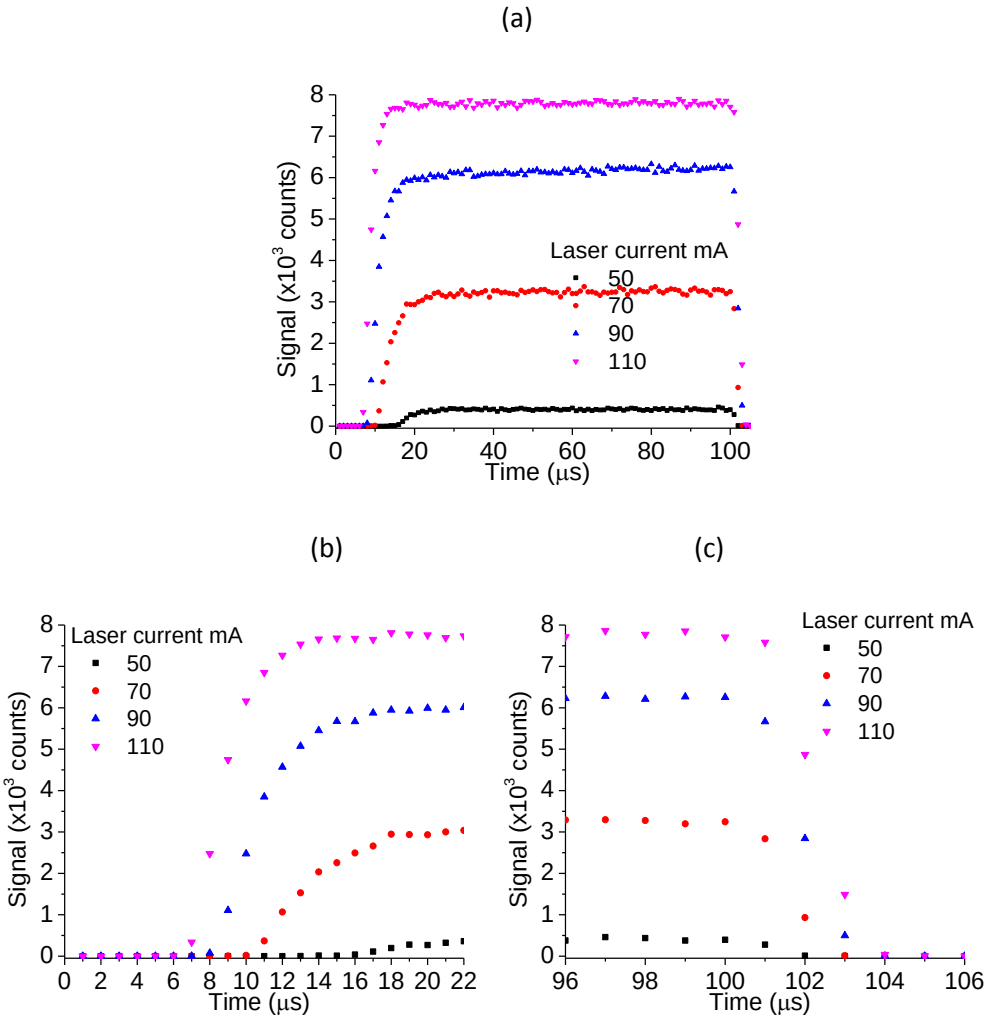

Figure 4-3. (a) Laser pulses, as measured using the PMT, for different laser powers (currents); (b) laser switch-on period; and (c) laser switch-off.

4.3 Stability test of the CryLas pulsed laser

To test the stability of the CryLas pulsed laser, the PMT was used as a detector. The PMT was placed in front of the dichroic mirror, which transmits only 5% of the total laser power. Additional neutral density filters and a variable aperture were used to avoid PMT saturation. The laser signal was integrated over one second.

Figure 4 shows the laser signal measured over 60 min and normalized to the mean signal. It was found that the standard deviation of the mean was <1 % the first 10 min, which is a typical patient treatment time. Over a 60-min period the fluctuations were within 2 %.

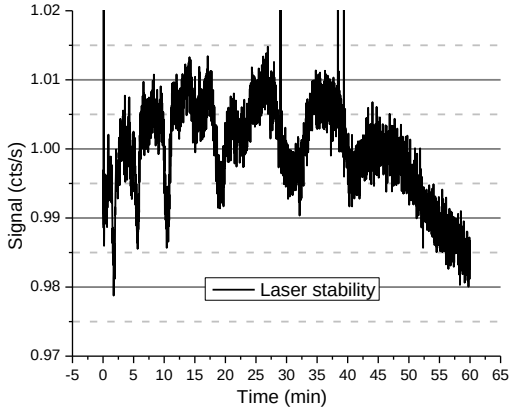

Figure 4-4. Laser signal measured for 1 h with 1 s integration normalized to the mean signal.

4.4 Test of PMT stability

Based on the fluctuation of the laser it was important to measure the fluctuation in the sensitivity of the PMT (Hamamatsu) as well. Thus, a constant light source was used and the signal from the PMT was measured over 2 h. Figure 4-5 shows the PMT signal from the light source measured over 2 h, normalized to the first measurement. The PMT tends to stabilize after ~ 1 h from a cold start. After the PMT stabilizes, the signal fluctuation was <0.5 %.

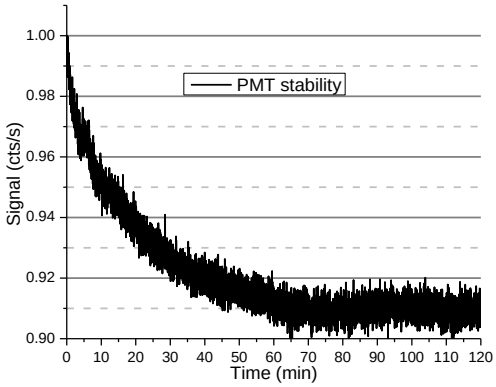

Figure 4-5. (a) PMT sensitivity variation measured using a constant light source. Each data point represents counts collected over a second; and (b) PMT signal normalized to the initial intensity.

4.5 Test of the RPL signal stability

To test the stability of the RPL signal from the RPLGD, two RPL samples (one un-irradiated and one irradiated with 10 mGy) were monitored in the system for ~ 8 min. The measurements were taken in the final setup with the pulsed laser (Section 4.1.2). For this, the measurements were started at the end of a laser pulse and the signal was collected for 100 µs. The signal at any given times was accumulated over 10000 laser pulses to improve the signal-to-noise ratio. The SR400 photon counter was set to add a delay of 2 µs after the laser trigger. A gate width of 5 µs was used to integrate the signal.

Figure 4-6a shows the RPL signal from an un-irradiated sample and the sample irradiated with 10 mGy. With this time-discrimination measurement, the signal for the sample irradiated with 10 mGy is already 6 times larger than the signal from the un-irradiated sample.

Figure 4-6b shows the RPL signal normalized to the mean signal over 8 min. It was found that the fluctuations were <1.5 % for both the un-irradiated and irradiated samples. This suggests that the observed instability is related to the instability from the laser observed in

Section 4.3. However, the variation in the laser intensity was approximately ±1 %, whereas we see a variation of approximately ±2% in the RPL signal. Therefore, there might be an additional cause of the fluctuations observed in the RPL signal. One possible explanation can be due to the jitter in the timing pulses of the SR400 photon counter. However, at this stage, the detailed causes remain unknown.

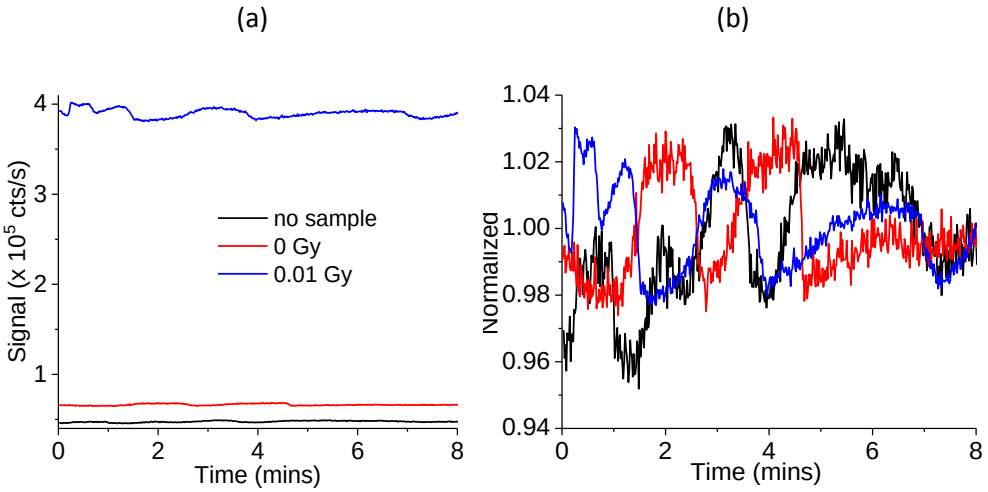

Figure 4-6. (a) Signal stability from glass rods that were un-irradiated and irradiated with 0.01 Gy. Background fluorescence signal (no sample) stability is also included for reference. (b) Signal normalized to the mean value from (a).

CHAPTER 5

BASIC MATERIAL CHARACTERIZATIONS

The objective of the studies in this chapter was to characterize the material properties of the silver-doped phosphate glass using the two custom built setups described in Sections 3.4.1 and 3.4.2. We investigated the luminescence centers, dose build up effect, the temperature dependence of the RPLGD. Optical absorption measurements were performed to find an optimum stimulation wavelength to potentially accelerate the build-up process.

The results show that the emission wavelength of the samples was different than the ones published in the literature. In addition, there is background fluorescence in the system, which affects the sensitivity and dynamic range of the system. The RPL of the material also exhibits a signal build up effect, and no other method was found to accelerate the build-up process, which leads to the conclusion that a correction algorithm must be developed. It was also found that the increase in temperature of the RPLGD and laser intensity reduces the RPL intensity with time.

5.1 Luminescence centers

The objective of this test was to study luminescence properties of the silver-doped glass samples used this study and compare to what has been reported in the literature so that we can optimize the components of the system including laser, optical filters etc. To achieve that, the emission spectra from an irradiated glass rod was collected with the USB-2000 Ocean Optics Spectrometer (Section 3.5.1). The stimulation source used here was the Thorlabs UV laser

(Section 3.4.1). A long pass 405 nm filter (25 mm diameter, model BLP01-405R-25, Semrock, Inc.) was used to cut off the laser emission. The spectra were corrected for the characteristics of the spectrometer grating and the response of the Ocean Optics spectrometer (Section 3.5.1).

Figure 5-1a shows the typical emission spectrum obtained from irradiated GD-300 glass. The two emission peaks from Ag^0 and Ag^{++} were observed at 450 nm and 630 nm, as mentioned in the literature. The emission is the same regardless whether we use beta sources or x-ray source (30 kV, 2.2 mA, 5 min exposures).

The observed luminescence emission spectrum, however, is not consistent with the published measurements. Kurobori et al. (2010) and Miyamoto et al. (2011) reported emission at ~450 nm and ~560 nm, where the 450 nm signal is non-radiation induced and the 560 nm signal is identified as the RPL signal. This inconsistency related to the PMT and spectrometer response in the measurement system used by these authors (Kurobori, Private Communication to Dr. McKeever). In another papper, Ihara et al. (2008) reported the RPL emission peak at 630 nm along with the dose independent PL peak at 450 nm, consistent with the current measurements.

The spectrum from Figure 5-1a was converted into an energy spectrum and fitted with three components as shown in Figure 5-1b. The fittings were performed in Origin 6.0 using their multi-peak fitting package. The measurements and fittings were found to be consistent with Fluorolog measurements as well.

It should be mentioned that the spectra were recorded with a constant wavelength bandwidth ($d\lambda$, in nm), not a constant energy bandwidth (dE, in eV). Therefore, when converting to display the result in terms of energy the intensity of the luminescence has to be corrected using the appropriate correction term, namely $(1/\lambda^2)d\lambda$.

Figure 5-1b shows that after fitting the emission spectrum has 3 bands. The main peak at ~630 nm consists of two bands at ~1.87 eV and ~1.93 eV whereas the third band is at ~2.62 eV.

In conclusion, detection of the RPL emission in a wide wavelength window from 600-700 nm should be used in the experimental fiber-based dosimeter system.

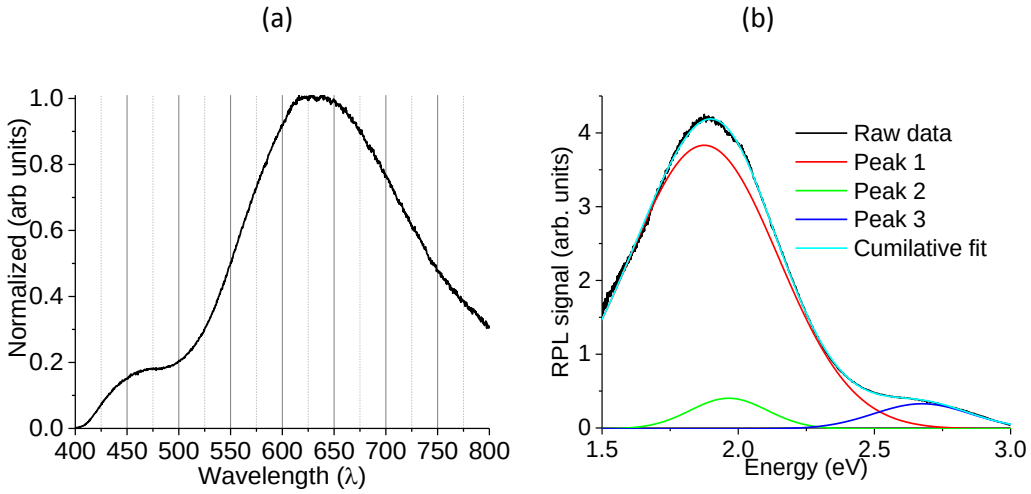

Figure 5-1. (a) Emission spectrum of silver-doped glass using a UV laser (375 nm) stimulation. The spectrum was recorded using a USB-2000 Ocean Optics spectrometer with 10 s integration time and averaging 5 acquisition. (b) Fit of the RPL spectrum from silver-doped glass with three Gaussian bands.

5.2 Background Fluorescence

5.2.1 Fluorescence spectrum

The system was found to have a high background fluorescence signal even without the RPLGD attached to the fiber. Figure 3-3 shows the components directly in the path of the laser light, which include convex lenses, a neutral density (ND) filter, a 375 nm laser line filter, the dichroic mirror, and the optical fiber. All have the potential to emit florescence if stimulated by

the UV laser. Thus, the following measurements were done to characterize the background fluorescence spectrum.

The spectrum of the system (no sample) was measured using a 405 nm long pass filter using the USB-2000 Ocean Optics spectrometer (Section 3.5.1). Figure 5-2 shows the measured background fluorescence spectrum. This emission is likely from the different optical components in the system. Additionally, it was found that any laser light that hits metallic surfaces also produces some fluorescence, probably caused by oxides on the surface of the metal. This light also has the potential to reach the photodetector.

To verify the emission spectrum indeed was from the setup, different materials were tested. It was found that different materials have different specific fluorescence emission spectra with different intensities. Figure 5-3 shows the background fluorescence spectrum from example materials with UV excitation. The cutoff at the ~405 nm is due to the use of a long pass 405 nm filter.

The system uses a 600 nm long-pass filter, which will reduce almost this entire fluorescence signal, but the problem will be the long tail extending beyond 600 nm to long wavelengths. This will overlap with the broad RPL emission and will reduce the signal-to-background ratio, thereby limiting the minimum detectable dose.

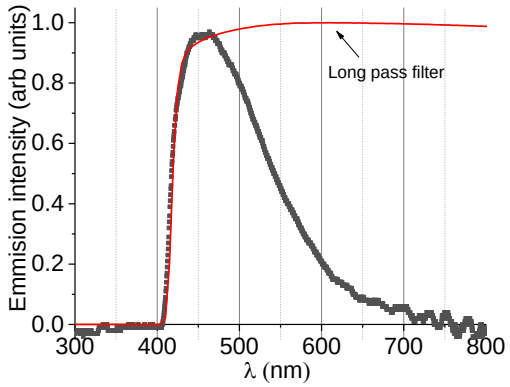

Figure 5-2. Background fluorescence spectrum from the optics used in the system. The spectra were recorded using the USB-2000 Ocean Optics spectrometer with 10 s integration time and averaging 5 acquisitions.

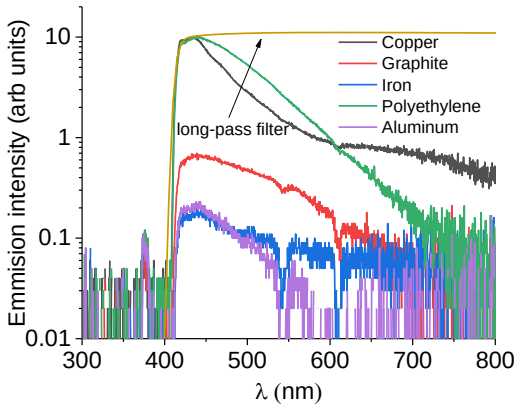

Figure 5-3. Background fluorescence spectrum from different materials with UV excitation. The spectra were recorded using the USB-2000 Ocean Optics spectrometer with 1 s integration time and averaging 5 acquisitions.

5.2.2 Background fluorescence stability

As the RPL signal from the samples will be on top of the background fluorescence signal, any fluctuations in the background signal would affect the RPL signal as well. Thus, the stability of the background fluorescence signal was investigated. For this, the background fluorescence signal was measured without any RPLGD in the system. The signals were integrated from 2 µs to 7 µs after each laser pulse with a total of 10,000 laser pulses, which is equivalent to 1 s integration time. Figure 5-4a shows the variation in the fluorescence signal over 10 min. This variation was found to be ~2%, which may be due to laser fluctuation. Thus, we can conclude that the background fluorescence signal from the system is stable.

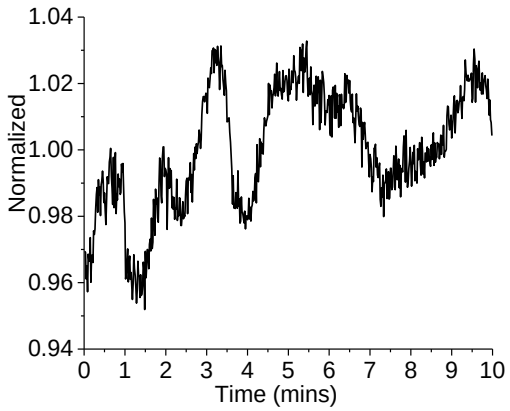

Figure 5-4. Stability of background flourescence signal over 10 min normalized to the mean signal.

5.2.3 Fluorescence lifetime

To characterize the properties of the background fluorescence signal from the system, its lifetime was determined using the system described in Section 3.4.2. The fluorescence was measured as a function of the delay between the laser pulse and the SR400 photon counting, as described in Section 3.4.3. The signals were integrated over multiples laser pulses to improve the SNR. The measurements were repeated five times for better statistics. The average of the five decay curves was fitted to obtain the fluorescence lifetime.

Figure 5-5 shows the fluorescence decay curve fitted with the double exponential function of type:

$$I = y_0 + \sum_{i=1}^{2} A_i \exp(-\frac{t}{\tau_i}) \qquad \textbf{(5-1)}$$

where τ_i's are the measured lifetimes for the *i*th signal. The fitted lifetime values showed that the background fluorescence signal has one fast component of lifetime <1 µs and slow component of lifetime ~ 11 µs. However, the limitation of the current setup was that the chosen window was 1 µs. Thus, the fast component of the lifetime cannot be resolved.

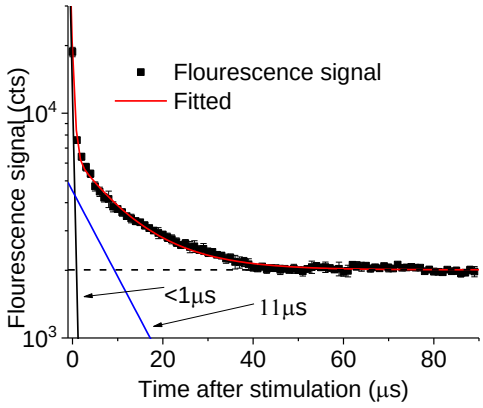

Figure 5-5. Background flourescence decay after the laser pulse. The measurements were repeated five times and the error bars in each data point represents the standard deviation between the readouts.

5.2.4 Fluorescence background as a function of laser intensity

To characterize the background fluorescence signal of the system as a function of laser intensity, the laser diode setup (Section 3.4.1) was used and the laser current was varied. Neutral density filters with total OD of 1.0 were used to avoid PMT saturation with the high laser current signal. The readout was performed in QCW mode with a laser pulse width of 0.1 ms and period of 1 ms. The SR400 photon counter was setup similar to the one as mentioned in lifetime measurements (Section 3.4.3) where the counter adds a 1 μs delay after the laser triggers using a gate width of 1 μs.

Figure 5-6a shows the fluorescence signal with time for different laser current. The fluorescence signal increases with increasing laser current, with the lifetime staying constant as seen in Figure 5-6b. In addition, the fluorescence signal increases linearly with laser current as shown in Figure 5-6c which was fitted with a linear function $y = ax + b$. Each data point represents the total counts from 104 μs to 155 μs and the error bars represent Poisson noise.

(a) (b)

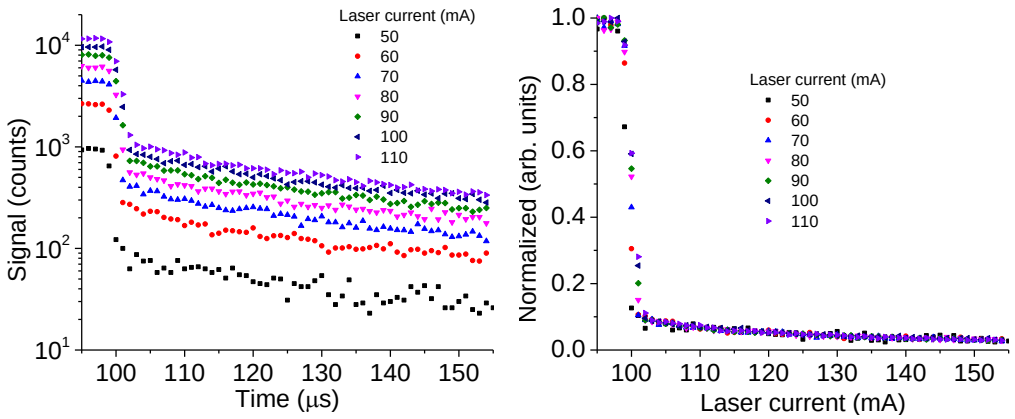

(c)

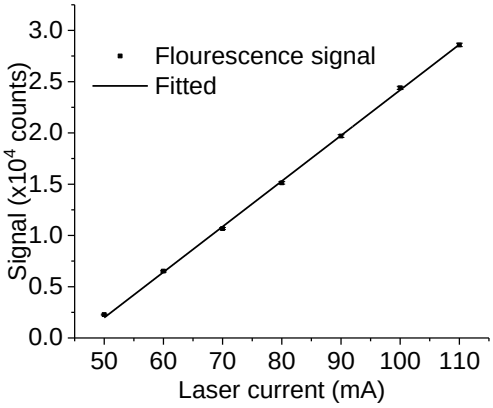

Figure 5-6. (a) Background fluorescence signal collected over time as a function of laser current with 100 μs laser pulse stimulation. (b) Normalized background fluorescence signal. The signal was normalized to the maximum fluorescence signal (during stimulation). (c) The linear dependence of background fluorescence signal with laser current. Each data point represents the total counts from 104 μs to 155 μs and the error bars represent Poisson noise.

5.3 Dose build-up effect

5.3.1 Characteristics

To test the build-up effect in the RPLGD, an un-irradiated sample was measured using the Ocean Optics spectrometer coupled to the in vivo dosimetry system. The spectrum was measured using a 405 nm long pass filter in front of the spectrometer. After the fluorescence

spectrum from the un-irradiated sample was measured, the sample was then irradiated with ~30 s beta dose. Immediately after the irradiation, the sample was placed back into the sample holder and the fluorescence spectrum was measured at different times.

Figure 5-7a shows the build-up effect in the silver-doped phosphate glass. The main RPL emission peak increases with time after irradiation, whereas the PL peak decreases within the first hour and stays constant. Figure 5-7b shows the peak intensity of the RPL signal increasing and the PL signal decreasing with time. Both the RPL and PL signal were normalized to their initial intensities. The observed build-up effect is identical to the one showed by Miyamoto et al. (2010a).

(a) (b)

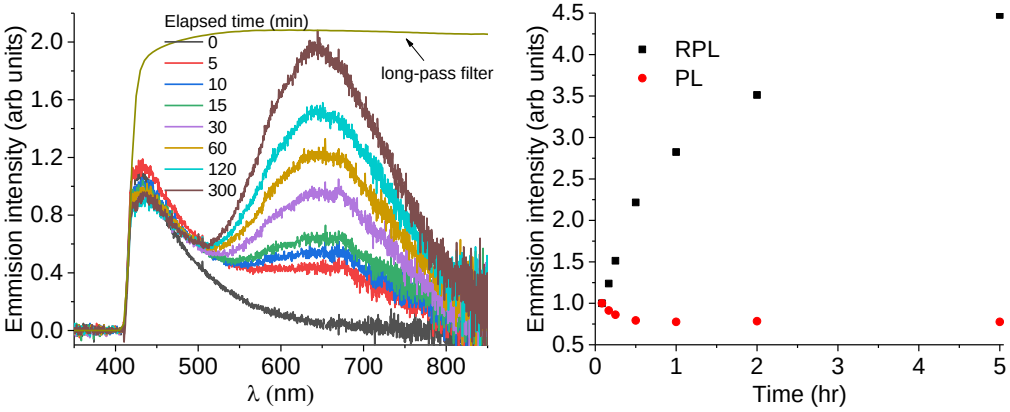

Figure 5-7. RPL build up from GD-450 glass following 30 s irradiation (^{90}Sr/^{90}Y beta). (a) The RPL emission spectrum as a function of time after irradiation. (b) The variation in RPL (600-700 nm) and PL (440-550 nm) emissions after the irradiation.

5.3.2 Optical absorption

It has been reported that heating accelerates the build-up effect. Chiyoda Dose Ace reader instruction recommends that the samples be heated at 70 °C for 30 min to accelerate the

build up. Because heating cannot be used to accelerate the build up of the RPLGD in vivo, optical absorption was measured to investigate the possibility of using optical stimulation to accelerate the build-up rate instead of using heat. Thus, optical absorption measurements were performed using the Cary 5000 spectrophotometer (Section 3.5.1) to find an optimum wavelength for excitation. The optical absorption of an un-irradiated silver phosphate sample (1 cm × 1 cm) was measured over the wavelength range of 200 nm to 800 nm. The same sample was then irradiated for ~ 30 min using the $^{90}Sr/^{90}Y$ beta source (dose of ~720 Gy). After irradiation, the sample was placed back in the sample holder and optical absorption measurements were carried out at different times after exposure.

Figure 5-8a shows the optical absorption spectrum of the un-irradiated sample along with the irradiated sample scanned at different times after exposure. The absorbance increases with time in the UV region due to the build-up phenomenon. Nevertheless, the optical absorption at a wavelength of ~ 350 nm – 410 nm and ~500 nm - 600 nm decreases.

Figure 5-8b shows the peak absorbances of the 530 nm and 390 nm bands decreasing with time. This shows that some of the centers that absorb at that wavelength are being reduced with time. This suggests that, if the RPLGD are stimulated with any of the two wavelengths, the build-up process may be accelerated. As 390 nm is close to the stimulation wavelength (355 nm), green stimulation (530 nm) was chosen to test build-up effect.

(a) (b)

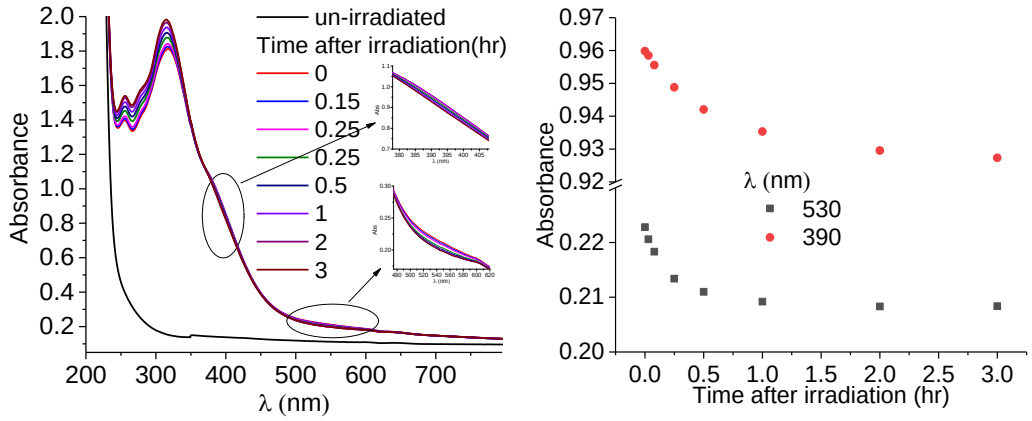

Figure 5-8. (a) Optical absorption spectrum during build of the RPL signal from an irradiated RPL glass and (b) peak absorbance as a function of time following irradiation.

Once the optimum wavelength was chosen, a green laser (100 mW output power, <1% stability, model GMLN-532-100FED, Lasermate Group, Inc.) was used as a stimulation source. After the laser stimulation, the RPL signal was measured using the Dose Ace system.

Six annealed RPL glass samples were used for this experiment. The first sample was irradiated for ~1 s using the beta source (dose of ~0.4 Gy). After irradiation, the sample was read using the Dose Ace System (Section 3.5.2) to take the first few measurements of the build up. Then the sample was then taken out and placed in front of the green (532 nm) laser for ~ 5 min (Section 3.6). After stimulating the sample for ~ 5 min, the RPL signal was read again using the Dose Ace System. This process was repeated for two more samples. As for the remaining three samples they were readout in a similar fashion, except that they were not stimulated with a green laser, but rather a 5 min wait added so that the samples would have similar build-up time of the first three samples.

Figure 5-9 shows the RPL signal between the samples with and without green stimulation after irradiation. It was found that the green stimulation did not accelerate the build-up rate, as the change in the RPL signal between the two sets are within uncertainties. In

addition to the green laser, yellow, red, infrared stimulation wavelengths were also tested as possible sources to accelerate the build-up rate. However, the change in the build-up rate was found within uncertainties.

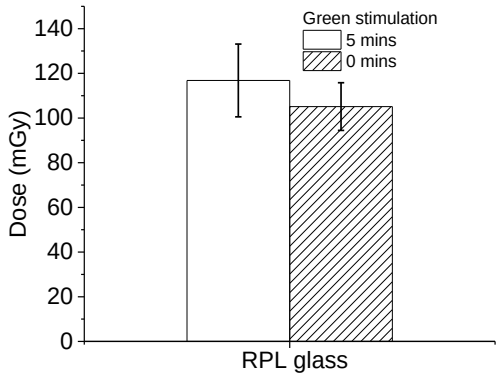

Figure 5-9. Effect of green stimulation during the build up of the RPL signal. The error bars represent the standard deviation between three samples.

5.3.3 Correction method

During in vivo measurements, post annealing of the sample is not possible, and no optical stimulation could be found to accelerate the build-up process. Thus, having a correction is essential to calculate dose by correcting the build-up effect. To develop this correction, however, characterization of the build-up rate is required. Thus, this experiment obtained to get build-up curves for different dose rates. The curves were fit with proper function to obtain the fitting coefficients, which can be later used to calculate dose from a sample based on the time of readout.

For this experiment, three annealed samples were taken and irradiated for ~ 1 s using the beta source (dose of ~0.4 Gy). Each sample was irradiated at different depths from the

source to get different dose rates. After each irradiation, the samples were read using the Dose Ace reader at different time intervals to obtain the build-up curve.

Figure 5-10 shows the build-up curve from the three samples irradiated with different dose rates. The curves were then fitted with three exponential of type:

$$I = y_0 + \sum_{i=1}^{3} A_i \exp(-\frac{t}{\tau_i}) \qquad \textbf{(5-2)}$$

where τ_i's are the measured lifetimes.

The fitted lifetime for each component are summarized in Table 3. The fitting coefficients for the fast lifetime are similar within uncertainties. For the long lifetime component, however, the lifetimes were significantly different. We believe this is due to lack of sufficient data points for longer times.

In conclusion, the build-up effect can be considered independent of the dose rate and dose thus, a universal build-up curve can be formulated and used to calculate dose from an irradiated sample based on the readout time.

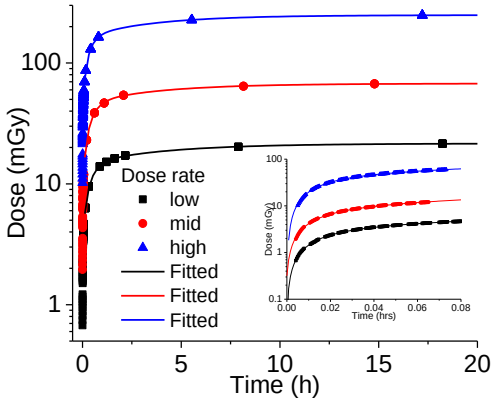

Figure 5-10. Build-up effect of the RPL signal fitted with an exponential.

Table 3. Fitting parameters from three different dose rates.

Dose rate(Gy/s)	τ1 (s)	τ2 (s)	τ3 (s)
Low	63± 2	1567 ± 15	16266 ± 316

Mid	60 ± 3	1587 ± 20	14835 ± 445
High	60 ± 1	1254 ± 6	14035 ± 74

5.4 Luminescence lifetime

Different authors have determined the luminescence lifetime of the 630 nm emission. Ihara et al. (2008) have determined the luminescence lifetime of RPL emission to be 3.8 – 4.3 μs and the PL emission 0.2-0.4 μs with 375 nm excitation. On the other hand, Kurobori et al. (2010) reported lifetimes of ~ 1.7 -3.6 μs for the RPL component and ~ 7 ns for the PL component for different doses with 340 nm stimulation. Thus, there are some discrepancies in the literature regarding the lifetime of the RPLGD. As our stimulation wavelength is 355 nm, the RPL and PL lifetimes was measured (Section 5.4).

For this, the RPL from three samples irradiated with ~ 10 mGy, 30 mGy, and 100 mGy were measured in the pulsed laser setup (Section 3.4.2). Figure 5-11 shows the time characteristics of the RPL signal of the irradiated and un-irradiated glass dosimeters. The RPL decay curves were then fitted with three exponential decay components. The fitted lifetime for each component are summarized in Table 4.

For all doses the lifetime of the RPL component was found to be ~ 3.5 μs. The additional two components with lifetime ~1 μs and ~11 μs are from the background fluorescence from the system.

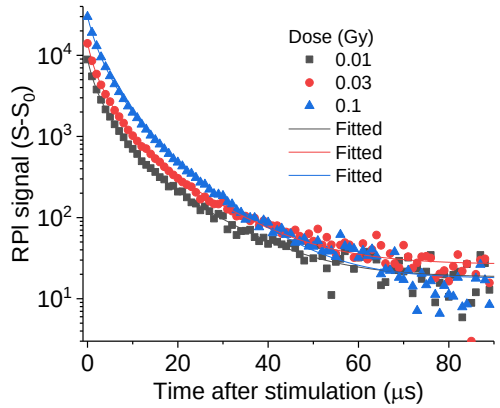

Figure 5-11. RPL lifetime measurements from irradiated RPLGDs.

Table 4. RPL lifetime components for different doses. The uncertaintites represented are fitting uncertainties.

Dose (Tölgyessy)	τ1 (μs)	τ2 (μs)	τ3 (μs)
0.01	1.02 ± 0.03	3.58 ± 0.16	11.7 ± 0.7
0.03	0.97 ± 0.02	3.46 ± 0.12	11.6 ± 0.6
0.1	1.17 ± 0.01	3.49 ± 0.07	10.1 ± 0.3

5.5 UV bleaching effect

Heating the glass at 400 °C for 20 – 60 min resets the samples (AGC Glass Corp, 2007). However, we observed that with UV stimulation the RPL signal can be bleached as well (Section 5.5).

To study this effect, nine samples were irradiated with the beta source for 1s , 2s , and 4s. After irradiation, the samples were heated at 70 °C for 30 min to accelerate the build-up effect. The samples were then read using the Dose Ace Reader. After readout, the samples were placed under a UV lamp with peak emission at 254 nm with an irradiance of 400 mW/cm^2 (Model 3UV-34 UV Lamp, output 4 W) for bleaching. The irradiance was measured using a power meter (Model 1918-C, Newport Corp.). After each exposure to the UV lamp, the samples were readout to measure the RPL signal depleted.

Figure 5-12a shows the RPL signal from samples irradiated with different doses decreasing each time after UV exposure. The rate of RPL signal depletion decreases with time as the rate of depletion coincides to the rate of build up. It was found that the rate of depletion was similar, independent of the dose delivered to the RPLGD. Figure 5-12b shows the rate of depletion of the RPL signal with UV exposure. Each data point is the average of the three samples for each dose and the error bars represent the standard deviation between them. We believe the uncertainties in the RPL signal might be due to uneven bleaching of the samples when placed under the lamp.

It was found that the rate of RPL depletion can be fitted with a double exponential decay function. At the end of the optical bleaching of the samples, the samples were annealed to 70°C to accelerate the build-up process and recover the original signal. However, it was found that only 50-60 % of the signal could be recovered.

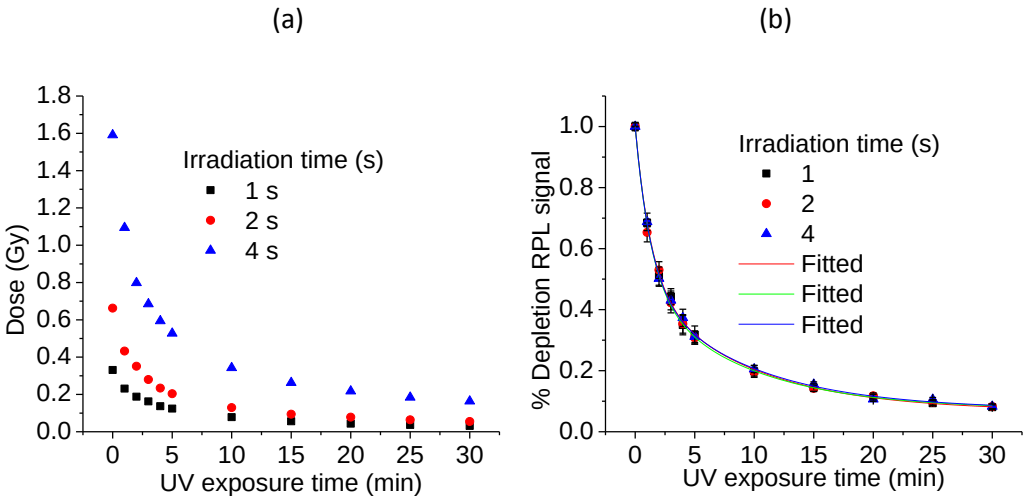

Figure 5-12. (a) RPL signal depletion with UV exposure times. (b) Rate of RPL signal depletion with UV exposure fitted with an exponential.

5.6 RPL signal response with laser intensity

To test the response of the RPL signal as a function of laser intensity, three samples (one un-irradiated and the other two irradiated with 0.01 Gy and 0.1 Gy) were examined using the laser diode setup (Section 3.4.1). During readout, the samples were placed at the end of the optical fiber. The readout was performed in Quasi-Continuous Wave (QCW) mode with a laser pulse width of 100 µs and period of 1 ms with maximum laser power. The RPL signals were recorded by adding a delay of 1 µs each time.

Figure 5-13a shows RPL signal from a 0.01 Gy sample collected over time with different laser stimulation current. The RPL signal increases with increasing laser current. In fact, the response is linear for all three samples (Figure 5-13b). Each data point represents the total counts integrated from 104 µs to 165 µs and the error bars represent Poisson noise. Low sensitivity was observed for the 0.01 Gy sample for lower laser currents below 110 mA. This is noticeable in Figure 5-13c, which shows the net RPL signal after background subtraction for 0.01 Gy and 0.1 Gy samples.

(a) (b)

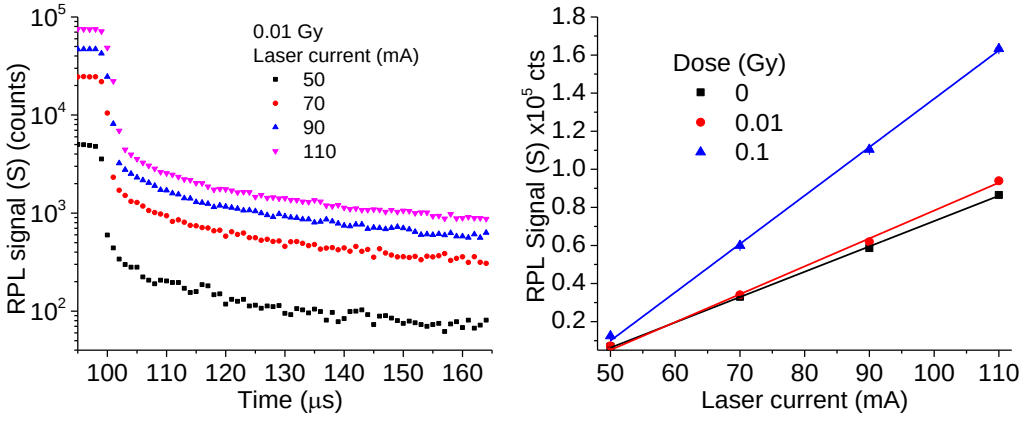

(c)

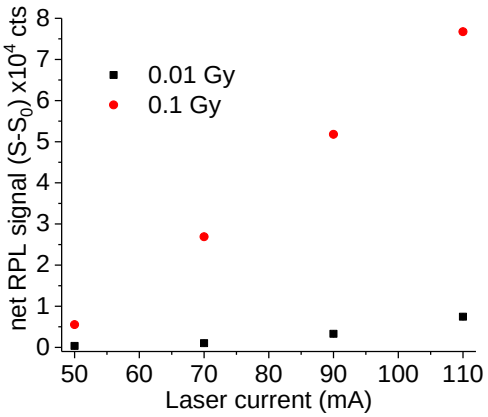

Figure 5-13. (a) RPL signal from 0.01 Gy sample collected over time as a function of laser current with 100 µs laser pulse stimulation. (b) RPL signal from the un-irradiated sample and with Each data point represents the total counts from 104 µs to 165 µs and the error bars represent Poisson noise. (c) The linear dependence of RPL signal ($S-S_0$) after subtraction of background signal with laser current.

5.7 Temperature effect

5.7.1 Laser intensity

The RPL signal from the glass was found to decrease over time with laser intensity. After cooling of the sample, the RPL signal returned to its initial intensity. We believe this happens due to the increase in temperature of the sample. After the laser is turned off, the sample starts to cool off and, hence, the signal increases again.

Thus, to characterize the effect of the laser intensity on the RPL signal, a sample irradiated with 100 Gy (beta) was readout in the laser diode setup (Section 3.4.1) in CW mode. The signals were recorded each second for 10 min. With time, the samples are believed to get heated due to laser stimulation and, hence, the signal starts to decrease.

Figure 5-14a shows the RPL signal decreasing over time with continuous laser stimulation with increasing laser current. The higher the laser current, the higher the RPL intensity, but also the higher the temperature dependence.

Figure 5-14b shows the RPL signal normalized to the initial intensity. It was found that with 110 mA laser current the RPL signal decreased to ~ 50% of its initial intensity, whereas with 50 mA laser current the RPL signal depleted to ~ 20% of its initial intensity. The reduction in the RPL signal with laser current was plotted and fitted with a single exponential function.

In conclusion, it was found that, with low laser current, the temperature dependence can be minimized with a loss in the signal response. In fact, with laser current lower than 35 mA the temperature dependence can be possibly eliminated. However, the current laser can only operate with laser current above 0.5 A thus, neutral density filters may be used to reduce laser power.

(a) (b)

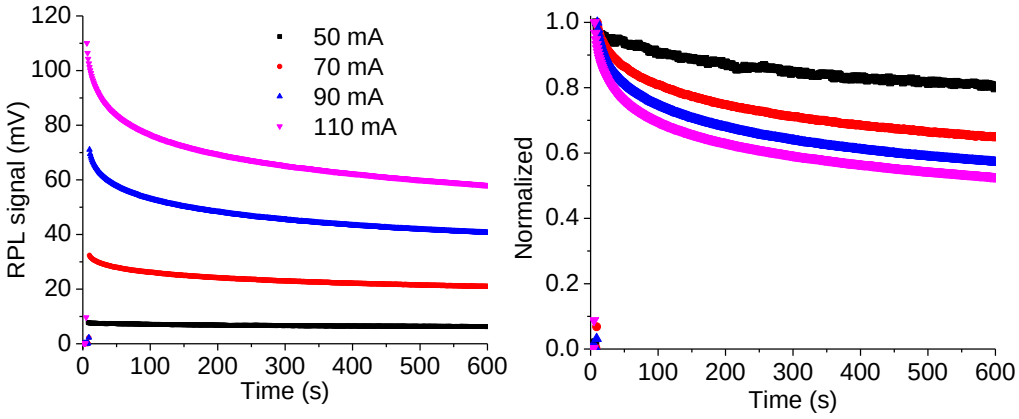

(c)

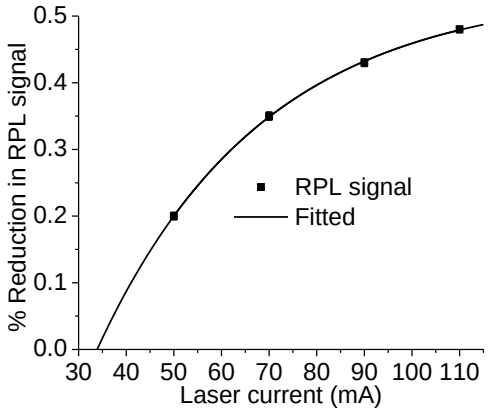

Figure 5-14. (a) Temperature dependence of the RPL signal for different laser current in CW mode. (b) RPL signal normalized to the initial intensity. (c) Total remaining RPL signal due to heating with laser stimulation after 10 minutes. The curve was fitted with one exponential. Ther error bars represent the standard deviation of three measurements.

5.7.2 Stimulation time

From the results of Section 5.7.1, it is clear that the RPL signal decreases with the laser power and the duration of the stimulation. Therefore, one would expect that this decrease is also dependent on whether the sample is read out using the laser operated in CW mode or in QCW mode since in the latter the stimulation time is reduced by a factor of 10 (0.1 ms pulse every 1 ms).

To test that, a sample irradiated with 3 Gy with 6 MV X-rays was read out using the laser diode setup (Section 3.4.1) in CW mode, and in QCW mode with 110 mA laser current. The signals were recorded every second for one minute.

Figure 5-15a shows the RPL signal decreasing over time in CW and QCW modes. As expected, the RPL signal decays more slowly in QCW mode than in CW mode. Figure 5-15b shows the RPL signal decay normalized to the initial intensity. It was found that in CW mode the RPL signal reduced by ~ 40%, whereas in QCW mode ~10% reduction was observed. Thus, with shorter stimulation pulses, the temperature dependence can be minimized.

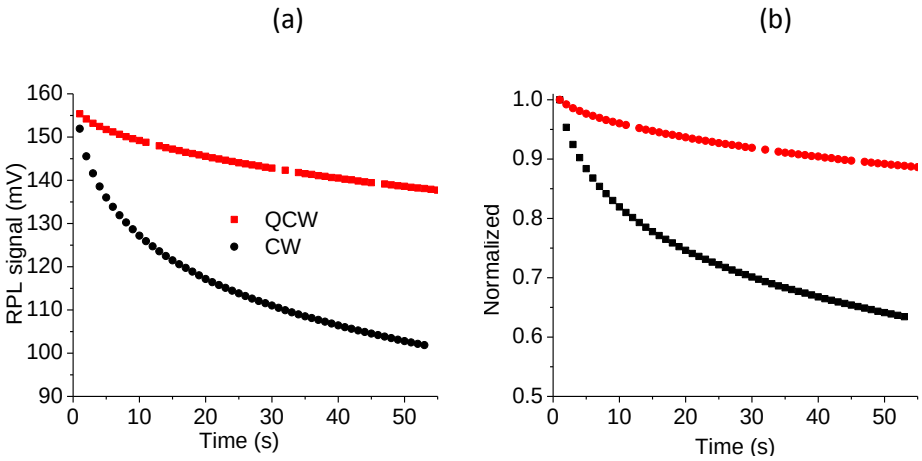

Figure 5-15. (a) Comparison of the temperature dependence of the RPL signal in CW and QCW mode. (b) RPL signal normalized to the initial intensity in CW and QCW modes.

CHAPTER 6

DOSIMETRY

The objective of the studies presented in this chapter was to characterize the dosimetric properties of the silver-doped phosphate glass using the two custom-built setups described in Sections 3.4.1 and 3.4.2. We performed dose response test using both setups using the samples irradiated with 6 MV X-rays (Section 3.3) to compare their sensitivity and performance. Preliminary measurements with the final setup were taken. Finally, based on the findings in Chapter 5 a qualitative model for the silver-doped glass was proposed.

The results show that the readout of the silver-doped glass with time discrimination method using a pulsed laser setup is better than the laser diode setup as most of the background fluorescence signal depletes in the first few μs increasing system's sensitivity.

6.1 Laser diode setup

6.1.1 CW mode and QCW mode (APD)

The dose response of the RPLGD was determined using the laser diode setup (Section 3.4.1). The signals were collected using an APD with the laser operating at 110 mA in CW mode and QCW mode. In QCW mode, a laser pulse width of 0.1 ms and period of 1 ms was used.

Figure 6-1a-c shows the RPL signal for the irradiated samples measured for 1 min. The temperature dependence can be observed during the sample readout, which resulted in a

reduction in signal, ~40% in CW mode and ~ 12% in QCW mode, over the readout period. This is because the net simulation time of the samples is less in QCW mode than in CW mode.

Figure 6-1b-d shows the dose response curve where each data point is the mean signal over the readout period and the error bars represent the standard deviation of the mean signal. The dose response was then fitted with a linear function $y = ax + b$ in linear scale and the intercept was set to zero. There are fluctuation in the mean signal in both CW and QCW mode. We believe this is due to the samples position reproducibility, since in this case the samples had to be removed and irradiated separately.

It was found that the RPL signal changes by about five orders of magnitude over the dose range investigated. The zero dose signal is ~ 1 mV in CW mode, equivalent to ~35 mGy, and ~1.5 mV in QCW mode, equivalent to ~ 30 mGy, if the response at 1 Gy is considered. Approximately 50% of this zero dose signal corresponds to the system background (no sample), where the system background signal is ~0.5 mV in CW mode, equivalent to ~15 mGy, and ~1 mV in QCW mode, equivalent to ~ 20 mGy.

In conclusion, QCW mode is better suitable for the RPL measurements as the temperature dependence is much less than that in CW mode.

(a) (b)

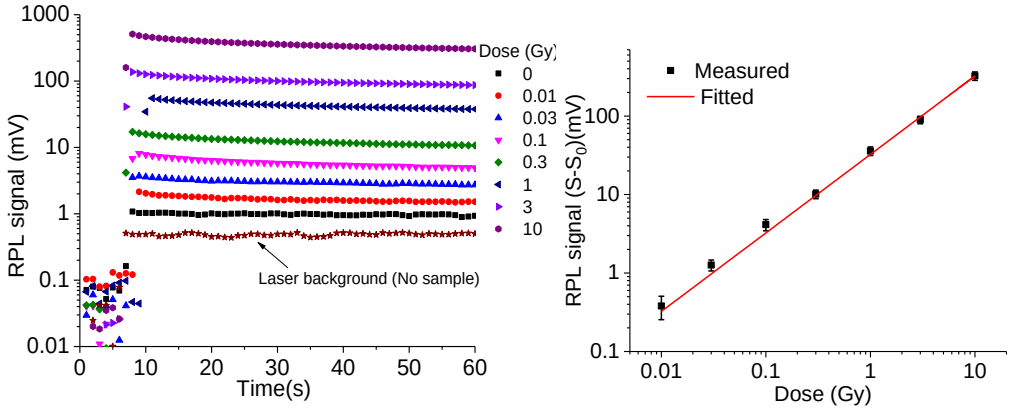

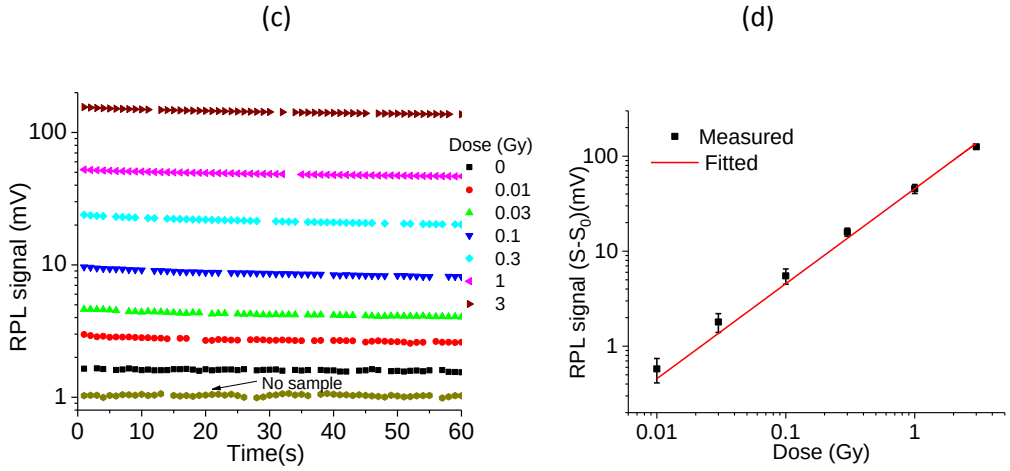

Figure 6-1. (a) RPL signal from samples irradiated with different doses. The lower signal in the initial region is when the laser was off. (b) Dose response curve where each data point is the mean signal over the reaout period. The error bars represent the standard deviation of the mean signal. (c) RPL signal from samples irradiated with Linac in QCW mode (0.1 ms pulse width and 1 ms period). Each data point is the average of the RPL signal from ~910 laser pulse of width 0.1 ms (for a 1 s). (d) Dose response curve where each data point is the mean signal and the error bars represent the standard deviation of the mean over the 60 measurements.

6.1.2 QCW mode (PMT)

To test the sensitivity of the system, a dose response was measured using the sample irradiated with doses from 10 mGy to 3 Gy by the 6 MV photon beam. During readout, the samples were placed at the end of the optical fibre. The readout was performed using the laser diode setup (Section 3.4.1) with the laser in Quasi-Continuous Wave (QCW) mode, with a pulse width of 0.1 ms and period of 1 ms with maximum laser power. Neutral optical density filters with a total OD of 1.3 were placed after the laser to avoid PMT saturation. The measurements were carried out using the SR400 photon counter with the timing parameters used in Section 3.4.3.

Figure 6-2a shows the total RPL signal with time for different doses. Figure 6-2b shows the dose response curve fitted with a linear function. The signal is integrated from 104 µs to 110 µs and the background signal (S_0) from the 0 Gy sample was subtracted. The error bars represent the propagated Poisson uncertainties after background subtraction. The fluctuation in the mean signal is due to samples position reproducibility, which can be improved in the final setup.

It was found that the background equivalent dose corresponds to ~35 mGy and minimum detectable dose (MDD) is ~ 3 mGy. However, we believe this can be improved with a pulsed laser setup. In addition, the dose response was not found to be linear. We believe this is due to background subtraction. The sample position was not very reproducible in the current system and, therefore, the signal measured from the un-irradiated sample may be higher than it actually is.

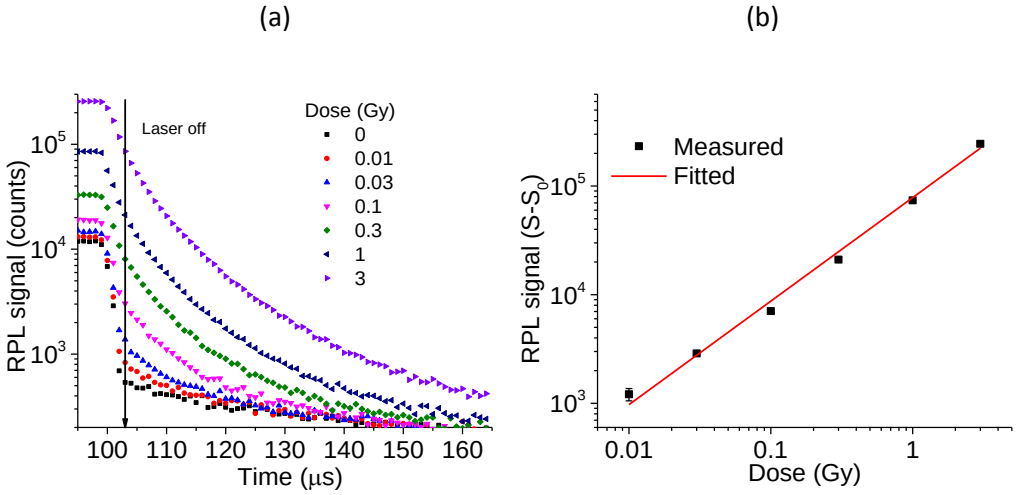

Figure 6-2.(a) RPL signal for different doses collected over time after 100 µs laser pulse stimulation. (b) Dose response curve obtained from the decay curves from (a) Each data point represents the total signal integrated from 104 µs to 110 µs after background subtraction. The error bars represent the propagated Poisson uncertainties after background subtraction.

6.1.3 Comparison of the QCW versus CW stimulation modes for sensitivity

We compared the sensitivity of the laser diode system using the two stimulation modes, QCW and CW. Samples irradiated with different doses using a 6 MV photon beams from a clinical accelerator (Section 3.3) were read using the laser diode setup (Section 3.4.1) operating in QCW mode. A laser pulse width of 0.1 ms and period of 1 ms with maximum laser current (110 mA) was used. Neutral density filters (OD of 1.3) placed after the laser to avoid PMT saturation. The measurements were carried out using the SR400 photon counter, with the timing parameters used in Section 3.4.3.

Figure 6-3a shows the total RPL signal with time for different doses. Figure 6-3b shows the comparison of the dose response curve with the laser on (CW mode) and Figure 6-3c shows the same after the pulse is switched off (pulsed mode). During stimulation, each data point represents the total signal from 95 μs to 99 μs, while after the pulse (Figure 6-3c) the signal is integrated from 104 μs to 110 μs. For both methods, the background signal from the 0 Gy sample was subtracted (i.e., RPL signal = $S-S_{o,}$ where S is the total signal and S_o is the background). The error bars represent the propagated Poisson uncertainties after background subtraction. It was found that the background equivalent dose and the minimum detectable dose is lower for the QCW mode than the CW mode. We believe this is due to the fast component of background fluorescence, which decays in time resolved measurement after the laser is switched off which reduces the background fluorescence signal from the system compared to the CW mode. Thus, QCW mode or time resolved measurement is better for RPL measurements than CW mode.

(a)

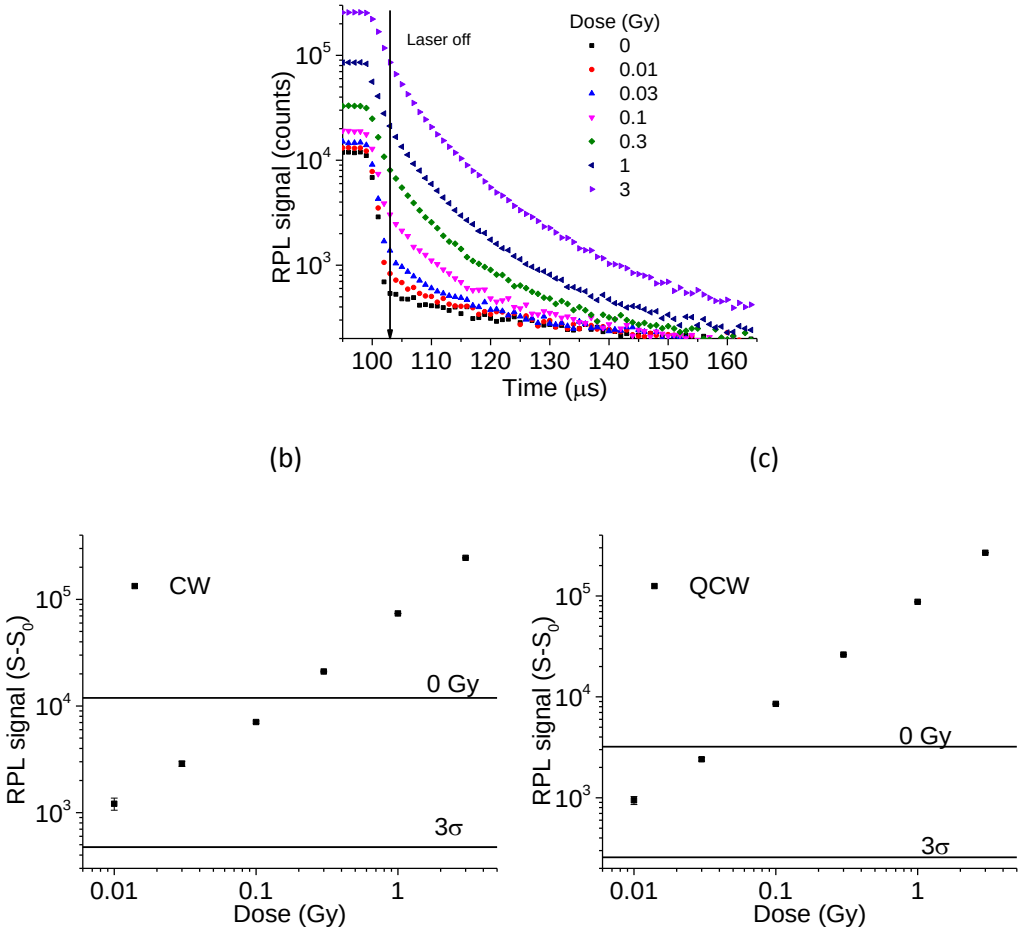

Figure 6-3. (a) RPL signals as a function of dose. (b) Dose response curves for RPL in CW mode. Each data point refers to the signal integrated over 95 μs to 99 μs during the stimulation pulse. (c) Dose response curves for RPL in QCW mode. Each data point refers to the signal integrated over 104 μs to 110 μs after the stimulation pulse (pulse mode). In both the dose response curves the zero dose signal (S_0) is subtracted, i.e. the RPL intensity minus the fluorescence background. Also shown in each plot are the background signal and a level corresponding to the 3x standard deviation of the background.

6.2 Pulsed laser setup

6.2.1 Dose response

We tested the sensitivity of the pulsed laser setup (Section 3.4.2). Samples irradiated with different doses using the 6 MV photon beams from a clinical accelerator (Section 3.3) were read in a similar way as described in Section 4.1.2.

Figure 6-4a shows the RPL decay curves for different doses, the RPL intensities increasing with increasing doses. The long decaying background signal, however, is the same for all RPLGD, irrespective of dose. Figure 6-4b shows the dose response curve fitted with a linear function passing through zero in the linear scale. Each data point represents the total RPL signal defined as the area under the curves in Figure 6-4a from 2 μs to 7 μs. The error bars represent propagated Poisson uncertainties after background subtraction. The maximum dose measured was 0.3 Gy, as the RPL signal from the 1 Gy sample saturated the PMT and, therefore, was not included in the dose response. The background equivalent dose is ~ 10 mGy, if the response at 0.1 Gy is considered.

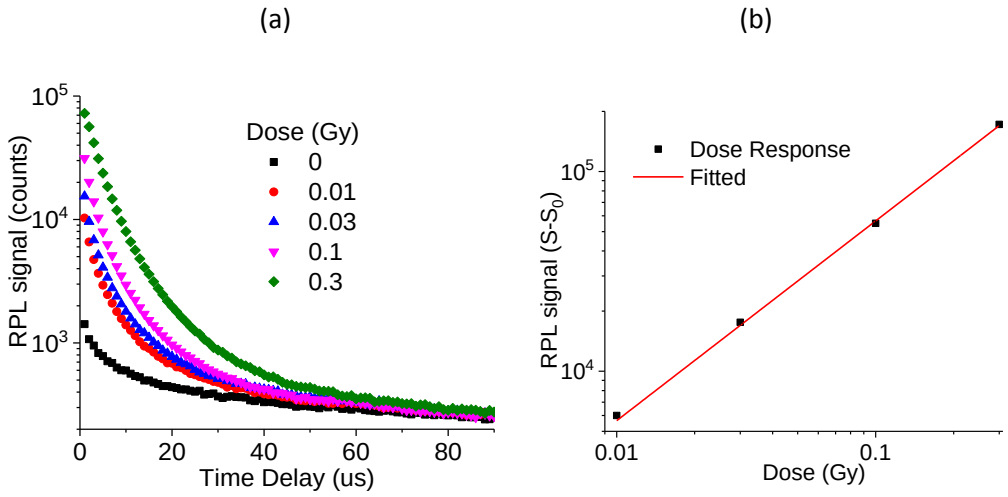

Figure 6-4. (a) RPL signal from samples irradiated with 6 MV X-rays and (b) Dose response curve, where each data point is the RPL signal integrated from 2 – 7 μs from (a) after background subtraction.

6.2.2 Preliminary measurements with beta source

To test the portable in vivo dosimetry system, four samples were annealed and irradiated using the beta source, individually, for 1, 2, 3, and 5 seconds. After irradiation, each sample was placed in the pulsed laser setup (Section 3.4.2) and read up to 200 s after irradiation. Thus, there is a time delay between irradiation and readout. During readout, the SR400 photon counter was set to add a delay of 2 μs and integrate signal for five μs. Thus, the RPL signal is integrated rom 2 μs to 7 μs. The T-counter was pre-set to count 10000 triggers so that counts will be accumulated for 0.5 s to improve the SNR. Figure 6-5 shows the RPL signal from the irradiated RPLGD. The signal keeps increasing after irradiation, which is the build-up effect (Section 5.3). However, the build up is higher for RPLGD irradiated with higher doses.

In conclusion, an algorithm that corrects for the build-up during irradiation is required to convert the RPL signal during the build up to dose.

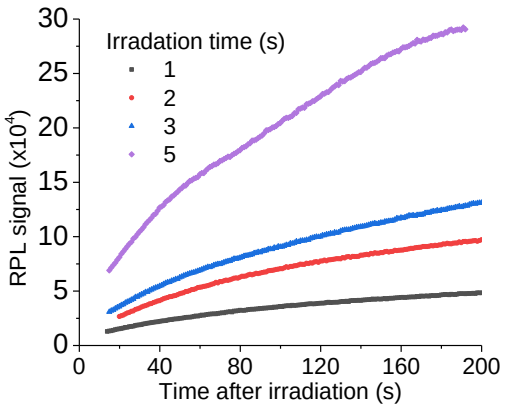

Figure 6-5. RPL signal from samples after irradiation (beta) and measured in the in vivo dosimetry system.

6.3 Proposed model

The current model of RPL emission for silver-doped phosphate glass proposed by Miyamoto et al. (2011) only explains the basic properties of the glass, such as the formation of RPL centers. When the glass is exposed to ionizing radiation, electron-hole pairs are produced. The liberated electrons and holes are then captured in the Ag^{+} sites, creating Ag^{0} and Ag^{++} ions. The author claims that the emission at 460 nm and 560 nm corresponds to the Ag^{0} and Ag^{++} (Section 2.4). Based on these emission bands the build-up effect in the glass has been explained by migration of holes trapped in the PO_4 tetrahedrons towards Ag^{+} ions to form Ag^{2+} ions (Perry, 1987). However, our observations show the main emission peak to be at ~630 nm (Section 5.1). In addition, it consists of two bands, which we believe are the Ag^{0} and Ag^{++} centers. Similar findings were observed with Electron Spin Resonance (ESR) studies of the silver doped phosphate glass by Yokota and Imagawa (1967). The third peak at ~450 nm is said to be due to Ag^{0} ions (Miyamoto et al., 2011), but we believe it is fluorescence signal from the sample not caused by the Ag^{0} center, since it does not increase with dose.

Therefore, the author's model qualitatively explains the dose build-up effect but a better model is required that explain other processes in the glass. In addition, in our experiments, we observed a series of findings, such as temperature dependence and UV bleaching effect, which are not explained by the current model as well. Thus, we expanded the model Miyamoto et al. (2011) to explain some of these effects.

During irradiation, the free electrons in the conduction band are trapped at the shallow traps. Perry (1987) also presented a model with the presence of an ineffective trap to explain the dose build-up effect. We believe this ineffective trap is a shallow trap. The presence of shallow traps is supported by TL measurements performed by Dr. Sergey Sholom (private communication) in which a broad temperature peak at ~ 90 °C, which increases with dose, was observed. Some of the electrons in the conduction band may also relax via an unknown "loss" pathway. This loss pathway could be deeper electron traps or recombination at unknown trapped hole centers.

Here speculate that the increase in concentration of both Ag^0 and Ag^{2+} centers is responsible for the build-up effect (Section 5.1). Immediately after radiation, the electrons from the valence band reach the conduction band and can be trapped in the shallow traps, whereas the holes are trapped in shallow hole traps. The buildup starts immediately with thermal stimulation of electrons from the shallow trap and holes from shallow hole traps at room temperature, which is a very slow process. This build-up process, however, can be accelerated with higher temperatures. During this thermal stimulation, some of the electrons and holes are lost via the unknown loss pathway, while others are trapped at Ag^+ converting them into the RPL centers, Ag^0 and Ag^{2+}. This causes the build-up in the RPL signal. The RPL signal reaches a maximum when the shallow traps have completely emptied.

UV bleaching effect was observed based on the findings in Section 5.5. During UV exposure (254 nm), electrons are excited from the RPL Ag^0 centers to the conduction band. The free electrons are retrapped in the shallow traps, but some can also be lost via the loss pathway. With the loss of electrons, the Ag^0 centers revert to Ag^+. When the UV light is turned off, the electrons from the shallow traps can get thermally stimulated. Again, some electrons are lost via the loss pathway, while other are trapped at Ag^+ centers converting these to Ag^0. Thus, the RPL signal builds up again, but now the maximum level is smaller than initially, due to electrons having been lost in the process. Thus, the UV effect is only partially reversible.

On the other hand, the temperature effect observed in Section 5.7 can be explained by thermal quenching phenomenon. Increasing the temperature during RPL measurements causes "thermal quenching" of the RPL signal. The sample can be heated either with a heater or with optical heating. During thermal quenching, the electrons do not get ionized to the conduction band. Thus, no electrons can be lost through the loss pathway, therefore; the decrease-increase cycle of the RPL signal is repeatable during the heating-cooling cycle.

The model proposed here is, at this point, speculative and will require more investigations to prove or disprove some of the processes proposed to explain the build-up effect and UV bleaching experiments.

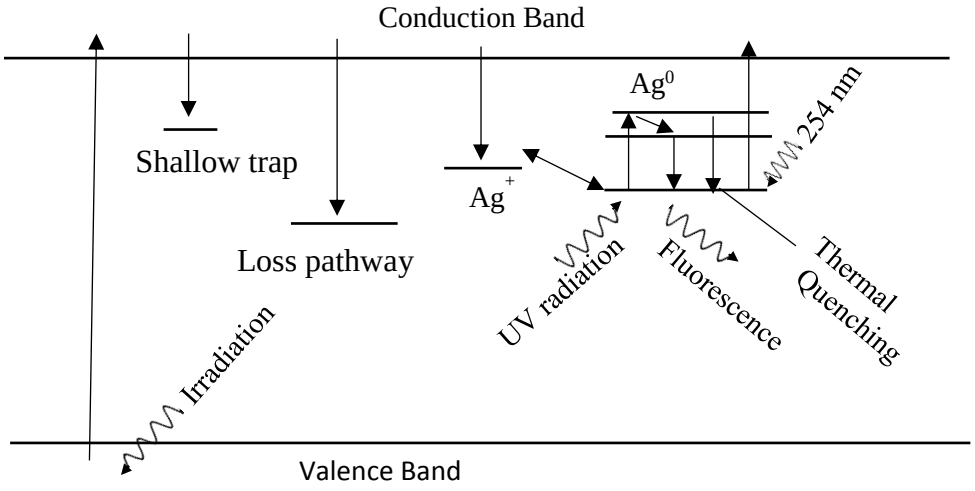

Figure 6-6. Proposed band diagram model for silver-doped phosphate glass.

CHAPTER 7

CONCLUSIONS AND FUTURE WORK

In this work, the potential of using the radiophotoluminescent (RPL) signal from the silver-doped phosphate glass for in vivo dosimetry was investigated, with the ultimate goal of developing a portable in vivo dosimetry system. Considerable effort was placed in designing and building various prototype configurations to test the components and carry out feasibility tests, as well as to identify potential obstacles. In addition, we also investigated the properties of the silver-doped glasses. The main setups investigated include a diode laser operated in both CW and QCW mode, and a pulsed laser. PMT and photodiodes were investigated as detection systems.

The results indicated that the diode laser when operated in QCW mode is limited by the laser rise and fall time, which needs to be taken in to account when taking time discrimination measurements. The PMT requires a warm up time of ~ 30 min to stabilize. The pulsed laser fluctuation is within 2% thus, monitoring the laser power is not necessary but may improve RPL signal reproducibility.

Based on the material characterization of the silver-doped glass, it was found that the emission wavelength of the samples was different than some of the results published in the literature. This discrepancy was explained by the possible differences in wavelength response of

the different systems. In our measurement, the emission was corrected by the spectral response of the system.

In addition, we identified background fluorescence in the system as one of the challenges to be solved. Considerable efforts were placed in trying to solve the system fluorescence problem and characterizing the contribution from different optical components. Unfortunately, there is no easy solution so far, and thus results this extra background component needs to be subtracted together with the pre-dose signal from the RPL signal. This reduces the sensitivity and dynamic range of the system. It was also found that the increase in temperature of the RPLGD and laser intensity reduces the RPL intensity with time. However, with use of proper neutral density filters this problem can be resolved.

A speculative model based on some of the new findings about the material has been proposed to explain build-up effect, which has not been satisfactorily explained in literature. In addition, to that, the model is able to explain the temperature dependence, UV bleaching effect which were not presented in literature or explained by previous models.

A primary challenge with using this technique in real time in vivo dosimetry is the well-known build-up effect of the RPL signal. The RPL signal increases continuously after irradiation and no other method (e.g. optical stimulation) was found to accelerate this process, which leads to the conclusion that a correction algorithm must be developed. The rate of build up was characterized and it was found to be independent of dose or dose rate. Thus, a universal build-up curve can in principle be formulated and used to calculate dose from an irradiated sample based on the readout time.

Future investigations can be divided into solving technical and methodological issues. As of the technical issues, the laser power needs to be monitored to account for any fluctuation in

the RPL signal. The sensitivity of the system with different length of optical fibers also needs to be tested. In addition, different RPLGD sizes should be investigated for in vivo measurements, as the crystals used in this study are probably too large for this application.

As for the methodological issues, in vivo measurements need to be taken with a clinical linear accelerator to characterize the build-up effect in conditions similar to the intended application. Based on this data, an algorithm must be developed to simultaneously convert the RPL signal into dose during the measurement.

REFERENCES

AGCGlassCorp, 2007. *RPL Glass Dosimeter / Small Element System: Dose Ace Technical Guide*.

Ahmed, M.F., Shrestha, N., Ahmad, S., Schnell, E., Akselrod, M.S. and Yukihara, E.G., 2017. *Demonstration of 2D dosimetry using Al2O3 optically stimulated luminescence films for therapeutic megavoltage x-ray and ion beams*. Radiat. Meas.

Araki, F., Ikegami, T., Ishidoya, T. and Kubo, H.D., 2003. *Measurements of Gamma-Knife helmet output factors using a radiophotoluminescent glass rod dosimeter and a diode detector*. Med. Phys. 30, 1976-1981.

Araki, F., Moribe, N., Shimonobou, T. and Yamashita, Y., 2004. *Dosimetric properties of radiophotoluminescent glass rod detector in high-energy photon beams from a linear accelerator and Cyber-Knife*. Med. Phys. 31, 1980-1986.

Aznar, M.C., Andersen, C.E., Bøtter-Jensen, L., Bäck, S.Å.J., Mattsson, S., Kjær-Kristoffersen, F. and Medin, J., 2004. *Real-time optical-fibre luminescence dosimetry for radiotherapy: physical characteristics and applications in photon beams*. Phys. Med. Biol. 49, 1655.

Beddar, A., Mackie, T. and Attix, F., 1992a. *Water-equivalent plastic scintillation detectors for high-energy beam dosimetry: I. Physical characteristics and theoretical considerations*. Phys. Med. Biol. 37, 1883.

Beddar, A.S., Mackie, T.R. and Attix, F.H., 1992b. *Cerenkov light generated in optical fibres and other light pipes irradiated by electron beams*. Phys. Med. Biol. 37, 925.

Bogdanich, W. and Series, U., *The New York Times; 2010*. West Virginia hospital over irradiated brain scan patients, records show.(March 6) Available from: http://www.nytimes.com/2011/03/06/health/06radiation.html.

Bogdanich, W. and Ruiz, R.R., 2010. *Radiation errors reported in Missouri*. New York Times, A17.

Brahme, A., 1984. *Dosimetric precision requirements in radiation therapy*. Acta Radiol. Oncol. 23, 379-391.

Cozzi, L. and Fogliata-Cozzi, A., 1998. *Quality assurance in radiation oncology. A study of feasibility and impact on action levels of an in vivo dosimetry program during breast cancer irradiation*. Radiother. Oncol. 47, 29-36.

Derreumaux, S., Etard, C., Huet, C., Trompier, F., Clairand, I., Bottollier-Depois, J.F., Aubert, B. and Gourmelon, P., 2008. *Lessons from recent accidents in radiation therapy in France*. Radiat. Prot. Dosim. 131, 130-135.

Duggan, D. and Coffey, C., 1998. *Small photon field dosimetry for stereotactic radiosurgery*. Med. Dosim. 23, 153-159.

Feldman, A. and Edwards, F.M., 2008. *1.11. The routine use of personal patient dosimeters is of little value in detecting therapeutic misadministrations*. Colin G. Orton and William R. Hendee, 51.

Gaza, R. and McKeever, S.W.S., 2006. *A real-time, high-resolution optical fibre dosemeter based on optically stimulated luminescence (OSL) of KBr:Eu, for potential use during the radiotherapy of cancer*. Radiat. Prot. Dosim. 120, 14-19.

Hendee, W., 2011. *Patient safety and the medical physicist*. Medical Physics-New York-Institute of Physics 38, i.

Hendee, W.R. and Herman, M.G., 2011. *Improving patient safety in radiation oncology*. Pract. Radiat. Oncol. 1, 16-21.

Howlett, S., Duggan, L., Bazley, S. and Kron, T., 1999. *Selective in vivo dosimetry in radiotherapy using p-type semiconductor diodes: A reliable quality assurance procedure*. Med. Dosim. 24, 53-56.

Huang, D.Y. and Hsu, S.-M., 2011. *Radio-photoluminescence glass dosimeter (RPLGD)*. In: Advances in Cancer Therapy. InTech.

IAEA, 2001. *Investigation of an accidental exposure of radiotherapy patients in Panama*. International Atomic Energy Agency.

Ihara, Y., Kishi, A., Kada, W., Sato, F., Kato, Y., Yamamoto, T. and Iida, T., 2008. *A compact system for measurement of radiophotoluminescence of phosphate glass dosimeter*. Radiat. Meas. 43, 542-545.

Ismail, A., Giraud, J.-Y., Lu, G.-N., Sihanath, R., Pittet, P., Galvan, J.-M. and Balosso, J., 2009. *Radiotherapy quality insurance by individualized in vivo dosimetry: State of the art*. Cancer/Radiothérapie 13, 182-189.

Jornet, N., Carrasco, P., Jurado, D., Ruiz, A., Eudaldo, T. and Ribas, M., 2004. *Comparison study of MOSFET detectors and diodes for entrance in vivo dosimetry in 18 MV x-ray beams*. Med. Phys. 31, 2534-2542.

Klein, D., Peakheart, D.W. and McKeever, S.W.S., 2010. *Performance of a near-real-time KBr:Eu dosimetry system under computed tomography x-rays*. Radiat. Meas. 45, 663-667.

Knežević, Ž., Beck, N., Milković, Đ., Miljanić, S. and Ranogajec-Komor, M., 2011. *Characterisation of RPL and TL dosimetry systems and comparison in medical dosimetry applications*. Radiat. Meas. 46, 1582-1585.

Kurobori, T., Zheng, W., Miyamoto, Y., Nanto, H. and Yamamoto, T., 2010. *The role of silver in the radiophotoluminescent properties in silver-activated phosphate glass and sodium chloride crystal*. Optical Materials 32, 1231-1236.

Lanson, J., Essers, M., Meijer, G.J., Minken, A.W., Uiterwaal, G. and Mijnheer, B.J., 1999. *In vivo dosimetry during conformal radiotherapy: requirements for and findings of a routine procedure*. Radiother. Oncol. 52, 51-59.

Lee, P.C., Sawicka, J.M. and Glasgow, G.P., 1994. *Patient dosimetry quality assurance program with a commercial diode system*. International Journal of Radiation Oncology* Biology* Physics 29, 1175-1182.

Maki, D., Nagai, T., Sato, F., Kato, Y., Yamamoto, T. and Iida, T., 2011. *Microscopic dose measurement with thin radiophotoluminescence glass plate*. Radiat. Meas. 46, 1543-1546.

Mangili, P., Fiorino, C., Rosso, A., Cattaneo, G.M., Parisi, R., Villa, E. and Calandrino, R., 1999. *In-vivo dosimetry by diode semiconductors in combination with portal films during TBI: reporting a 5-year clinical experience*. Radiother. Oncol. 52, 269-276.

Mijnheer, B., Beddar, S., Izewska, J. and Reft, C., 2013. *In vivo dosimetry in external beam radiotherapy*. Med. Phys. 40, 070903-n/a.

Miyamoto, Y., Yamamoto, T., Kinoshita, K., Koyama, S., Takei, Y., Nanto, H., Shimotsuma, Y., Sakakura, M., Miura, K. and Hirao, K., 2010a. *Emission mechanism of radiophotoluminescence in Ag-doped phosphate glass*. Radiat. Meas. 45, 546-549.

Miyamoto, Y., Kinoshita, K., Koyama, S., Takei, Y., Nanto, H., Yamamoto, T., Sakakura, M., Shimotsuma, Y., Miura, K. and Hirao, K., 2010b. *Emission and excitation mechanism of radiophotoluminescence in Ag+-activated phosphate glass*. Nuclear Instruments and Methods in Physics Research Section A: Accelerators, Spectrometers, Detectors and Associated Equipment 619, 71-74.

Miyamoto, Y., Takei, Y., Nanto, H., Kurobori, T., Konnai, A., Yanagida, T., Yoshikawa, A., Shimotsuma, Y., Sakakura, M., Miura, K., Hirao, K., Nagashima, Y. and Yamamoto, T., 2011. *Radiophotoluminescence from silver-doped phosphate glass*. Radiat. Meas. 46, 1480-1483.

Mizuno, H., Kanai, T., Kusano, Y., Ko, S., Ono, M., Fukumura, A., Abe, K., Nishizawa, K., Shimbo, M., Sakata, S., Ishikura, S. and Ikeda, H., 2008. *Feasibility study of glass dosimeter postal dosimetry audit of high-energy radiotherapy photon beams*. Radiother. Oncol. 86, 258-263.

Perks, J., Gao, M., Smith, V., Skubic, S. and Goetsch, S., 2005. *Glass rod detectors for small field, stereotactic radiosurgery dosimetric audit*. Med. Phys. 32, 726-732.

Perry, J.A., 1987. *RPL Dosimetry, Radiophotoluminescence in Health Physics*. CRC Press.

Rah, J.-E., Kim, S., Cheong, K.-H., Lee, J.-W., Chung, J.-B., Shin, D.-O. and Suh, T.-S., 2009. *Feasibility study of radiophotoluminescent glass rod dosimeter postal dose intercomparison for high energy photon beam*. Appl. Radiat. Isot. 67, 324-328.

Rah, J.-E., Hwang, U.-J., Jeong, H., Lee, S.-Y., Lee, D.-H., Shin, D.H., Yoon, M., Lee, S.B., Lee, R. and Park, S.Y., 2011. *Clinical application of glass dosimeter for in vivo dose measurements of total body irradiation treatment technique*. Radiat. Meas. 46, 40-45.

Rah, J.-E., Oh, D.H., Shin, D., Kim, D.-H., Ji, Y.H., Kim, J.W. and Park, S.Y., 2012. *Dosimetric evaluation of a glass dosimeter for proton beam measurements*. Appl. Radiat. Isot. 70, 1616-1623.

Ramsey, C., Dube, S. and Hendee, W.R., 2003. *It is necessary to validate each individual IMRT treatment plan before delivery*. Med. Phys. 30, 2271-2273.

Ramsey, C.R., Seibert, R., Mahan, S.L., Desai, D. and Chase, D., 2006. *Out-of-field dosimetry measurements for a helical tomotherapy system*. Journal of Applied Clinical Medical Physics 7, 1-11.

Saini, A.S. and Zhu, T.C., 2004. *Dose rate and SDD dependence of commercially available diode detectors*. Med. Phys. 31, 914-924.

Sato, F., Zushi, N., Sakiyama, T., Kato, Y., Murata, I., Shimizu, K., Yamamoto, T. and Iida, T., 2015. *Radiophotoluminescence light scope for high-dose dosimetry*. Radiat. Meas. 82, 88-92.

Scalchi, P. and Francescon, P., 1998. *Calibration of a MOSFET detection system for 6-MV in vivo dosimetry*. International Journal of Radiation Oncology* Biology* Physics 40, 987-993.

Schulman, J.H., Ginther, R.J., Klick, C.C., Alger, R.S. and Levy, R.A., 1951. *Dosimetry of x-rays and gamma-rays by radiophotoluminescence*. J. Appl. Phys. 22, 1479-1487.

Son, K., Jung, H., Shin, S.H., Lee, H.-H., Kim, M.-S., Ji, Y.H. and Kim, K.B., 2011. *Evaluation of the dosimetric characteristics of a radiophotoluminescent glass dosimeter for high-energy photon and electron beams in the field of radiotherapy*. Radiat. Meas. 46, 1117-1122.

Thwaites, D.I., Mijnheer, B. and Mills, J.A., 2005. *Quality assurance of external beam radiotherapy*.

Tölgyessy, J., 1991. *CRC Handbook of Radioanalytical ChemistryVolume 1*.

Van Dam, J. and Marinello, G., 1994. *Methods for in vivo dosimetry in external radiotherapy*. Garant Publ.

Vatnitsky, S., Lopez, P.O., Izewska, J., Meghzifene, A. and Levin, V., 2001. *The radiation overexposure of radiotherapy patients in Panama 15 June 2001*. Radiother. Oncol. 60, 237-238.

Yamamoto, T., 2011. *Rpl dosimetry: Principles and applications*. In: AIP Conf. Proc., AIP, 217-230.

Yokota, R. and Imagawa, H., 1967. *Radiophotoluminescent centers in silver-activated phosphate glass*. J. Phys. Soc. Jpn. 23, 1038-1048.

VITA

NISHAN SHRESTHA

Candidate for the Degree of

MASTERS OF SCIENCE

THESIS: DEVELOPMENT OF AN IN VIVO DOSIEMETRY SYSTEM USING RADIOPHOTOLUMINESCENCE FROM SILVER DOPED PHOSPHATE GLASS FOR RADIOTHERAPY APPLICATIONS

MAJOR FIELD: PHYSICS

BIOGRAPHICAL: PERSONAL
Born in Chitwan, Nepal on April 08, 1990

EDUCATION

BACHELOR OF SCIENCE 2013
Southern Arkansas University, Magnolia, AR

EXPERIENCE

RESEARCH ASSISTANT 2013 – 2016
Oklahoma State University, Stillwater, OK

TEACHING ASSISTANT 2016 – 2017
Oklahoma State University, Stillwater, OK